Chapter 4

Cu(II), Ni(II) and Co(II) Pyrimidine Schiff base complexes

4.1. Introduction

Pyrimidine derivatives and heterocyclic annulated pyrimidines continue to attract great interest due to their wide variety of interesting biological activities such as anticancer, antiviral, antitumor, anti-inflammatory and antimicrobial activities. The pyrimidine ring is found in vitamins like thiamine, riboflavin and folic acid. Barbitone, the first barbiturate hypnotic sedative and anticonvulsant is a pyrimidine derivative. Pyrimethamine, a selective inhibitor of the DHFR of malarial plasmodia antimalarial drug combined with sulfonamide sulphadiazine is used for treating HIV positive individuals. Trimethoprim- antibiotic used in the treatment of urinary tract infections. Methotrexate and aminopterin are both used in cancer chemotherapy.

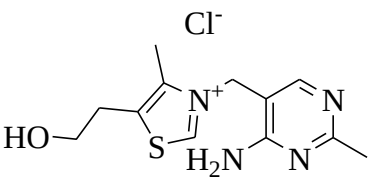

Thiamine

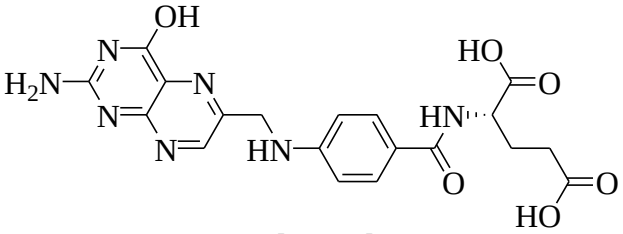

Folic acid

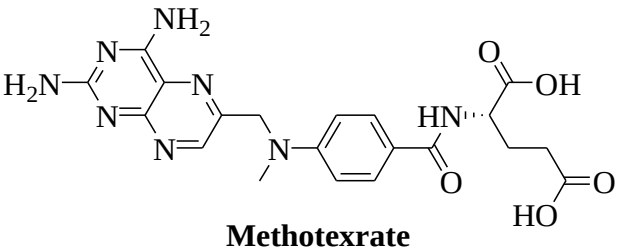

Methotexrate

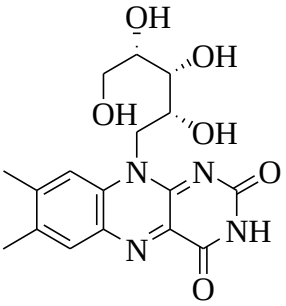

Riboflavin

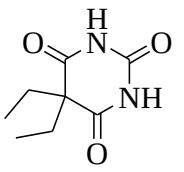

Barbitone

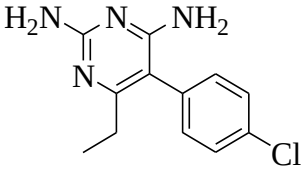

Pyrimethamine

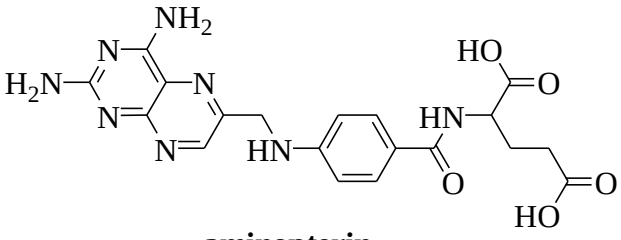

aminopterin

It is well-documented that pyrimidine derivatives play a significant role in many biological systems, the ring system being components of nucleic acids, several vitamins, co-enzymes *etc.*, provide potential binding sites for metal ions. Moreover, pyrimidine analogues have the capacity to impede the bio-synthesis of pyrimidine nucleotides. Certain drugs with pyrimidine rings are employed in the treatment of neoplastic diseases and infections caused by fungi and DNA containing viruses. On the other hand, biguanides and guanyl ureas which have attracted much attention because of their well-acclaimed medicinal values (*e.g.*, anti-malarial activity of paludrine) are also well established as coordinated agents. In the living systems, biguanide is known to undergo cyclisation to form triazine which is the active substance to act as anti-malarial drug. It was therefore considered necessary to study some pyrimidine derivatives with the hope that the resulting compounds might have biological potency and to evaluate the coordination pattern of such ligands by complexation with metal ions in order to understand more precisely the role of such metal ions in living systems.

Schiff bases exhibit useful biological activities such as anti-inflammatory, analgesic, anti-microbial, anti-convulsant, anti-tubercular, anti-cancer, anti-oxidant, anthelmintic, anti-glycation and anti-depressant activities. Schiff bases are also used as catalysts, pigments and dyes, intermediates in organic synthesis, polymer stabilizers and corrosion inhibitors. Pyrimidine derivatives and heterocyclic annulated pyrimidines continue to attract great interest due to their wide variety of interesting biological activities such as anti-cancer[1,2], anti-viral[3], anti-tumor[4,5], anti-inflammatory[6,7] and anti-microbial activities[8,9]. Schiff bases attract much interest both from a synthetic and biological point of view[10, 11]. Most of the reports in the literature

reveal that Schiff bases derived from various heterocyclic compounds possess cytotoxic[12, 13], anti-convulsant, anti-proliferative [14, 15], anti-microbial [16, 17] and anti-cancer[18] activities. They also show activity against gonadotropin releasing hormone receptors as well as herbicidal activity targeting acetohydroxyacid synthase, which catalyze the first common step in branched-chain amino acid biosynthesis. Furthermore, many pyrimidine-5-carbonitrile derivatives are proved to exhibit potent anticancer as well as antimicrobial activities. Patients with neo-plastic disorders are mostly subjected to microbial infections. The co-administration of multiple drugs for treating patients suffering from cancer disease accompanied with microbial infections might inflect some added health problems, especially in patients with impaired liver and/or kidney functions. Therefore, the concept of monotherapy by a single drug which possesses dual utility might be advantageous from both therapeutic as well as cost-effective stand points. Consequently, our efforts were devoted to synthesize and investigate innovative pyrimidine analogs with dual function; anticancer/antimicrobial. Aligned with this scope, we synthesized some pyrimidine Schiff bases bearing biologically active functionalities and studied their biological activity in detail, which we report in this chapter.

4. 2. Experimental work

The instruments used to characterize these ligands and the complexes, methods used for pharmacology are already discussed in section 3.2 and 3.3.

4. 2.1. Synthesis of ligands

A mixture of 5,6-diamino-2-mercapto-*1H*-pyrimidin-4-one (0.15 g, 1 mmol), salicylaldehyde (0.12 ml, 1 mmol) or 5-bromo salicylaldehyde (0.20 g, 1 mmol) in 95% ethanol was refluxed for 2 h. The precipitate was filtered and washed with ethanol.

4.2.1.1.*6-amino-5-[2-hydroxy-benzylidene)-amino]-2-thioxo-tetrahydro-pyrimidin-4-one(1)L*^{1} :

Yellow colour crystals, Crystallized from DMF/H_2O; yield 78%; m.pt: 237 °C. Anal. calcd (%) for $C_{14}H_{19}N_5O_3S$ (334.38) C, 49.84; H, 5.68; N, 20.76; found (%), C, 49.79; H, 5.63; N, 20.70, IR(cm^{-1}): 1554(C=N); 1354(C=S), UV-vis(nm): 310, 415. ^{1}H-NMR(ppm): δ6.76-8.15(m, 4H, aromatic); δ7.86(s, 1H, -CH=N), δ8.11(s, -CH=N,1H, pyrimidine ring), δ11.57(-NH_2, 2H,pyrimidine ring).

4.2.1.2.*6-amino-5-[2-bromo-6-hydroxy-benzylidene)-amino]-2-thioxo-tetrahydro-pyrimidin-4-one(2)L^2* :

Yellow colour crystals, Crystallized from DMF/H_2O; yield 75%; mp: 254 °C. Anal.calcd for $C_{14}H_{18}BrN_5O_3S$ (414.29) C, 40.39; H, 4.36; N: 16.82; found, C, 40.31; H, 4.29; N: 16.76. IR(cm^{-1}): 1560(C=N); 1357(C=S), UV-vis(nm): 325, 420.^{1}H-NMR(ppm): δ6.85-8.45(m, 4H, aromatic); δ7.93(s, 1H, -CH=N), δ8.52(s, -CH=N,1H, pyrimidine ring), δ11.71(-NH_2, 2H,pyrimidine ring).

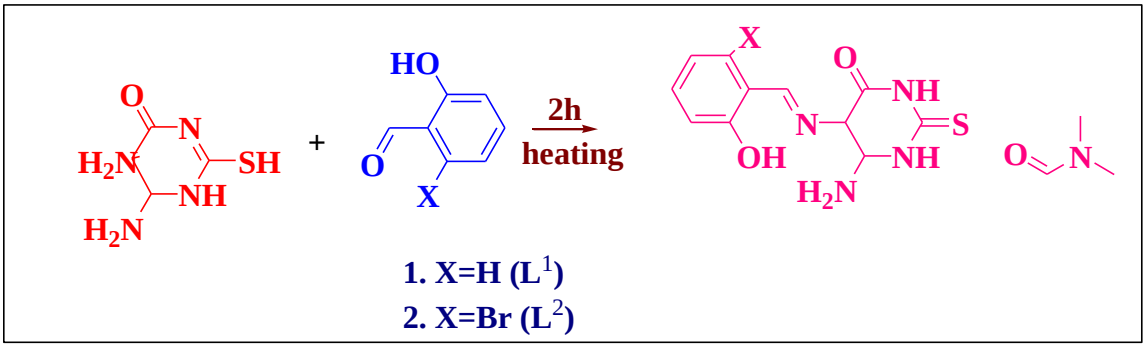

Scheme 1: Synthesis of the ligands

4.2.2 Synthesis of complexes

4.2.2.1. Synthesis of [Cu(L^1)(ONO$_2$)] (3) and [Cu(L^2)(ONO$_2$)] (4)

A methanolic solution (20 mL) containing **1** (0.334 g, 1mmol) or **2** (0.414g, 1 mmol) and copper nitrate (0. 2g, 1mmol) were added and refluxed for 5h. The resulting mixture was then cooled to room temperature, which resulted in the formation of brown coloured precipitate. It was filtered off and the solid was recrystallised from ethanol and then subjected to purification by TLC. Our efforts to obtain single crystal of the complexes were unsuccessful. Brown coloured crystalline precipitate was obtained. Yield: 65%. m.pt: 251-254°C. Anal. calcd (%) for $C_{14}H_{17}N_6CuO_6S$: C, 36.48; H, 3.72; N, 18.23, S, 6.96. Found (%): C, 36.36; H, 3.75; N, 18.16; S, 6.84. Anal. calcd.(%) for $C_{14}H_{16}N_6CuO_6SBr$: C, 31.15; H, 2.99; N, 15.57. Found(%): C, 31.18; H, 2.90; N, 15.50.

4.2.2.2. Synthesis of [Ni(L^1)(ONO$_2$)] (5) and [Ni(L^2)(ONO$_2$)] (6)

It was prepared using the same procedure as described for **3** and **4** with **1** or **2** and nickel(II) nitrate(0.2g, 1mmol). Red coloured precipitate. Yield. 74%. m.pt: 257-259°C. Anal. calcd.(%) for $C_{14}H_{17}N_6NiO_6S$: C, 36.87; H, 3.76; N, 18.43, S, 6.99. Found (%): C, 36.79; H, 3.71; N, 18.45; S, 6.99. Anal. calcd. (%) for

$C_{14}H_{16}N_6NiO_6SBr$: C, 31.43; H, 3.01; N, 15.71. Found (%): C, 31.39; H, 2.96; N, 15.70.

4.2.2.3. Synthesis of $[Co(L^1)_2]$ (7) and $[Co(L^2)_2]$ (8):

It was prepared using the same procedure as described for **3** and **4** with L^1 **(1)** or L^2 **(2)** and cobalt(II) chloride(0.2g, mmol). Brown coloured crystalline precipitate was obtained. Yield: 76%. m. pt: 253-259°C. Anal. calcd (%) for $C_{28}H_{36}CoN_{10}O_6S_2$: C, 45.96; H, 4.96; N, 19.14; S, 8.76; Found (%): C, 45.85; H, 3.85; N, 15.75; S, 7.21. Anal. calcd (%) for $C_{28}H_{34}Br_2CoN_{10}O_6S_2$: C, 37.81; H, 3.85; N, 15.75; S, 7.21; Found (%): C, 37.79; H, 3.80; N, 15.69; S, 7.15.

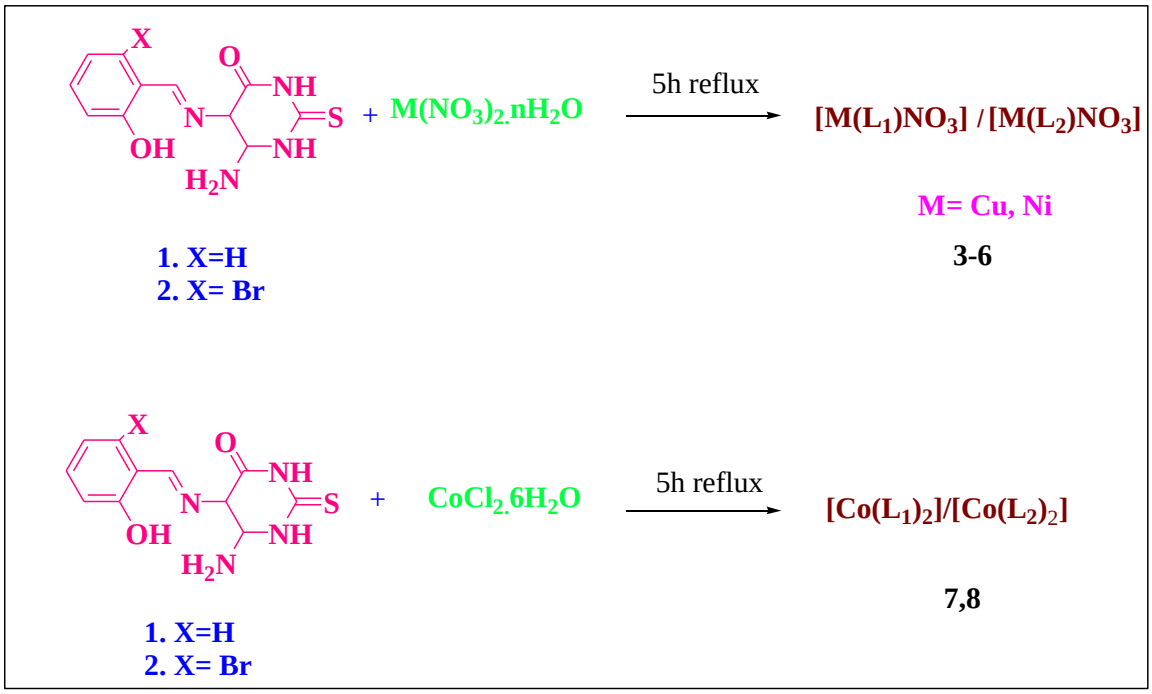

Scheme 2: Synthesis of the complexes

4. 3. Characterization of ligands and complexes

The synthesized ligands and the complexes have been characterized using various spectral techniques like FT-IR, UV-visible, NMR, Single crystal XRD, EDAX and TGA.

4.4. Determination of X-Ray crystal structure

A Bruker *APEX-2* X-ray (three-circle) diffractometer was employed for crystal screening, unit cell determination and data collection. The X-ray radiation employed was generated from a *Mo* sealed X-ray tube (Kα= 0.7017Å with a potential of 40 kV and a current of 40 mA) fitted with a graphite monochromator in the parallel mode (175 mm collimator with 0.5 mm pinholes). Systematic reflection conditions

and statistical tests of the data suggested the space group P121/c1. A solution was obtained readily using *SHELXTL (XS)*. Hydrogen atoms were placed in idealized positions and were set riding on the respective parent atoms. All non-hydrogen atoms were refined with anisotropic thermal parameters[19]. The structure was refined (weighted least squares refinement on F^2) to convergence. Olex-2 was employed for the final data presentation and structure plots[20]. Supplementary material for the crystal structure has been deposited with the Cambridge Crystallographic Data (CCDC no: 1012277**(1)** and 1048130**(2)**; deposit@ccdc.cam.ac.uk or http://ccdc.cam.ac.uk).

4. 5. Results and discussion

Analytical data indicated the formation of 1:1 and 1:2 metal complexes with ligands **1** and **2** respectively with Cu(II), Ni(II) and Co(II) metal ions. The Schiff bases were soluble in ethanol and methanol. All the metal complexes were coloured, non hygroscopic solids, stable in air, infusible at higher temperature, insoluble in water and many common organic solvents but they are soluble in DMF and DMSO. The molar conductance values of the complexes (measured in 10^{-3}M DMF) are in the range of 1.5–3.6 Scm^2 mol^{-1} indicating their non-electrolytic nature.

4.5.1. Structural description of the ligand

The synthesis of the Schiff bases was performed as shown in scheme 1. The single crystal XRD studies of the Schiff base ligand **1** shows that the compound **1** has the empirical formula $C_{14}H_{16}N_5O_3S$ with formula weight 334.38. It crystallizes in the monoclinic crystal system with the space group P121/c1 having unit cell dimensions a=13.079(3), b=13.785(3), c=8.5074(19) Å and β=95.395(3)°. The bond lengths of S(1)–C(2), O(2)–C(3), N(4)–H(4A), N(4)–H(4B), N(5)–C(12), and N(5)–C(13) are 1.6693(15), 1.2336(18), 0.9000, 0.9002, 1.3276(19), 1.453(2) Å respectively. The bond angles of H(4A)–N(4)–H(4B), C(1)–N(4)–H(4A), C(1)–N(4)–H(4B), N(1)–C(2)–S(1), N(2)–C(2)–S(1), C(9)–C(8)–H(8) are 108.1, 119.5, 11.0, 121.06, 123.96, and 120.2 respectively. Hydrogen bonds are formed between O3–H and N3, O2 and H5, N4–H and O4, and N1–H and O4. The ORTEP diagram of the Schiff bases **1** and **2** are shown in Fig. 4.1 and 4. 2 respectively. The single crystal XRD of the Schiff base **2** shows that the empirical formula is C_{14} H_{16} Br N_5 O_3 S with formula weight 414.29. It crystallizes in the monoclinic crystal system with the unit cell dimensions a=14.343(2) Å, b=14.114(2) Å, c=8.2728(13) Å, β=94.955(2)° with space group P121/c1. The bond lengths for Schiff base 2 are Br(1)–C(8), S(1)–C(1), O(1)–C(2),

N(1)–H(1), N(3)–C(4), C(2)–C(3), C(6)–C(7), C(13)–H(13A), and C(14)–H(14A) are 1.9026 (15), 1.6692 (15), 1.2318 (18), 0.8800, 1.3275 (18), 1.4342 (19), 1.405 (2), 0.9800, and 0.9800 respectively. The bond angles are C(11)–O(2)–H(2), C(1) –N(1)–H(1), C(1)–N(1)–C(2), C(4)–N(3)–H(3B), N(1)–C(1)–S(1), C(9)–C(8)–Br(1), and C(8)–C(9)-H(9) are 109.5, 116.8, 126.50 (12), 119.1, 123.76 (11), 119.21 (11) and 120.1 respectively.

The crystal data and the structural refinement parameters are given in Table 4.1. The selected bond lengths and bond angles for ligands **1** and **2** are given in Table 4.2 to Table 4.4 respectively. The packing diagram of the Schiff bases **1** and **2** are shown in Figs. 4.1a and b respectively.

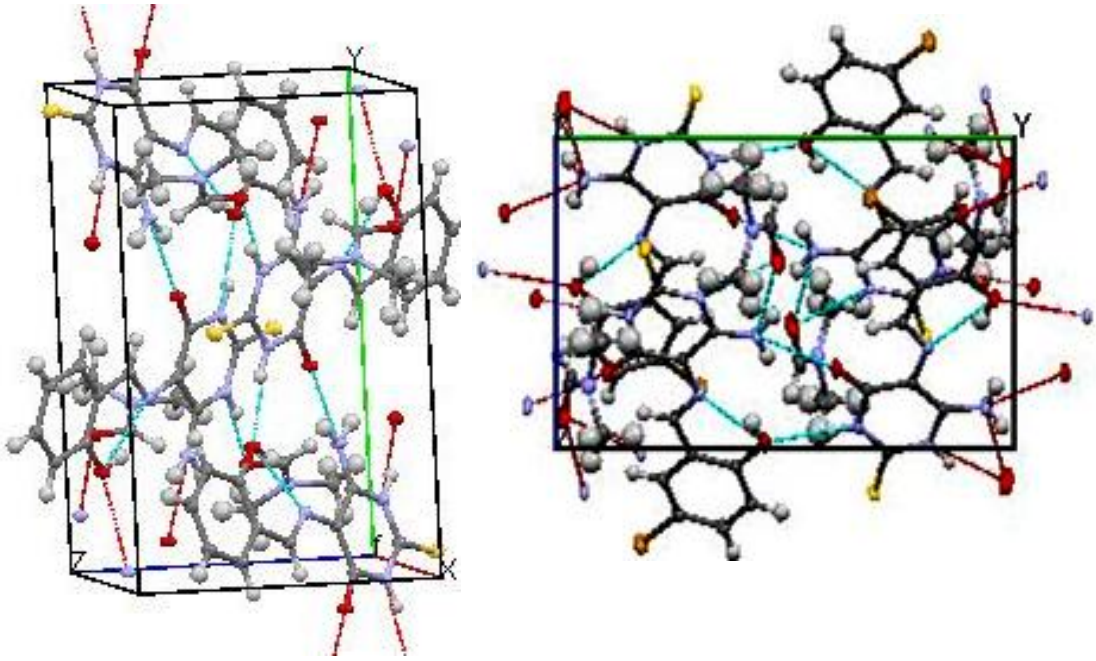

Fig. 4.1a and b. Packing diagram of the Schiff bases 1 and 2

The hydrogen bonding existing between the compounds are shown in the packing plot. The hydrogen bonds exist between the primary amino hydrogen and the oxygen of the dimethyl formamide solvent molecule. Another hydrogen bond exist between N(1), NH in the pyrimidine ring and O(4), oxygen of the solvent DMF molecule.

4.5.2. Infrared Spectra

The characteristic IR bands of the ligands **1** and **2** were assigned at 3201, 3363cm^{-1} and 3223, 3369cm^{-1} to –NH_2 stretching frequencies respectively. The stretching frequencies for C-H pyrimidine at 3065 and 3113cm^{-1}, CH=N at 1554 and

1560 cm^{-1}, C=O in pyrimidine at 1657 and 1729 cm^{-1} for Schiff bases **1** and **2** respectively**.**

The IR spectra of the complexes were compared with that of the free ligand to show the changes during complexation. The IR spectra of the Cu(II) complexes **3** and **4**, showed a broad band around 3430 to 3234 cm^{-1} due to the amine and the lattice water peaks. The γ(C=N) stretching vibration, in the free ligand at 1554 and 1560 cm^{-1} for **1** and **2** has been shifted to 1520 and 1511 cm^{-1} proving that the azomethine nitrogen is involved in co-ordination. The band at 1729 and 1657 for **1** and **2** which are responsible for the carbonyl group in the pyrimidine ring vanished in the IR spectrum of Cu(II) complexes showing that the group has been enolised and that is proved from the broad band in the region 3057 to 3430cm^{-1}. The C-O stretching frequency in **1** and **2** are 1104 and 1100cm^{-1} which is shifted to higher wavelengths in the complexes 1139 and 1136 cm^{-1} showing that the phenolic –OH is involved in co-ordination.

In the Ni(II) complexes **5** and **6** the bands are isostructural with Cu(II) complexes and it can be visualized in Table 4.5. In the Co(II) complexes, the primary amino stretching frequencies appeared around 3200-3500cm^{-1} , the bands are shifted to a small extent and the presence of the primary amine bands proved that the $–NH_2$ group has been involved in co-ordination. The shift in the azomethine nitrogen confirmed its co-ordination with the metal. The >C=O stretching frequency appeared at 1725 and 1656cm^{-1} confirming the enolisation is absent in Co(II) complexes.

The important IR stretching frequencies of the ligand and the complexes are given in Table 4.5. The non-ligand bands around 1300-1316cm^{-1} in the complexes **3-6** show that the nitro group is co-ordinated in a unidentate fashion except Co(II) complexes. The FT-IR spectrums of the ligand and the complexes are shown in Figs. 4.3a-h.

The C=S stretching frequency appeared around 1353-1355cm^{-1} for ligand **1** and its complexes **(3, 5, 7)** and 1346-1358 cm^{-1} for ligand **2** and its complexes **(4,6,8)** proving the absence of coordination of the sulfur atom to metal ion. The IR spectra of all the complexes show two absorption bands in the far infrared region, 420-440 cm^{-1} and 480-520 cm^{-1}, which are assignable to (M-O) and (M-N) vibrations, respectively. The absence of water molecules inside the coordination sphere of the Co(II) and Ni(II) complexes was confirmed from the absence of additional band at 860 cm^{-1} in

the IR spectra of the complexes suggesting that water molecules are not coordinated to the metal ions[21-23].

Table 4. 5. FT-IR stretching frequencies of the ligand and the complexes in cm^{-1}

Compounds	FT-IR stretching frequencies(cm^{-1})				
	$-NH_2$/-OH	**C=O**	**C=N**	**C-O**	**C=S**
L^1	3201,3363	1729	1556	1104	1354
L^2	3223,3369	1657	1546	1100	1357
$[Cu(L^1)(ONO_2)]$	3065-3350	-	1520	1139	1355
$[Cu(L^2)(ONO_2)]$	3005-3370	-	1511	1136	1358
$[Ni(L^1)(ONO_2)]$	3086-3370	-	1522	1137	1353
$[Ni(L^2)(ONO_2)]$	3085-3380	-	1513	1138	1358
$[Co(L^1)_2]$	3229,3361	1725	1531	1112	1354
$[Co(L^2)_2]$	3311,3363	1656	1525	1119	1356

4. 5. 3. Electronic spectra

The electronic spectra of the ligands **1** and **2** show bands at 240- 260 and 300-360 nm. The first band corresponds to the π→π* transition and band at 300-360 nm corresponds to n→π* transition associated with the >C=N and >C=S functional groups of the Schiff bases.

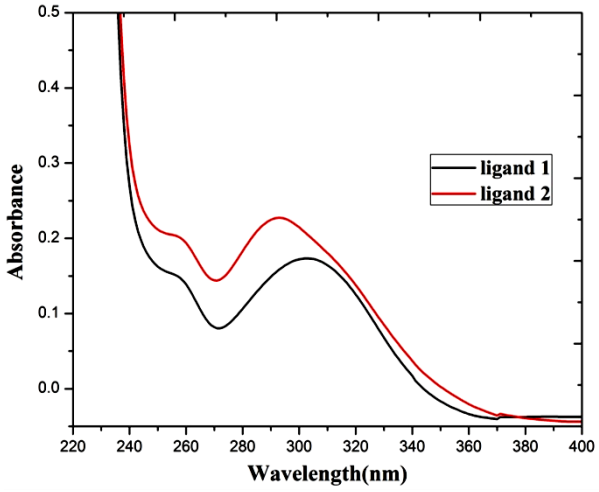

Fig. 4. 4a. Electronic spectrum of the ligands

The electronic spectra of **3** and **4** are an indication of four co-ordinate square planar geometry for Cu(II). The bands from 220 nm to 280 nm in the complexes may be assigned to intra ligand charge transfer transitions. The divalent copper with $3d^9$ electronic configuration is subject to Jahn-Teller distortion and hence, regular octahedral complexes cannot be expected. However, tetrahedral Cu(II) complexes are rare because of Jahn-Teller effect, which causes a flattening of tetrahedron due to lifting of the degeneracy $^2T_{2g}$ ground state. The electronic spectrum of the Cu(II) complexes are shown in Fig 4. 4b, c and d respectively. The electronic bands around 400-500 nm is due to the two transitions $^2B_{1g} \rightarrow {}^2A_{1g}$ ($d_{x2-y2} \rightarrow d_{z2}$), $^2B_{1g} \rightarrow {}^2B_{2g}$ ($d_{x2-y2} \rightarrow d_{zy}$) and the band at 285nm is due to the charge transfer transitions. The Cu(II) complex is paramagnetic (μ_{eff}=1.79 BM) confirming the presence of one unpaired electron. The electronic spectral details are given in Table 4.6.

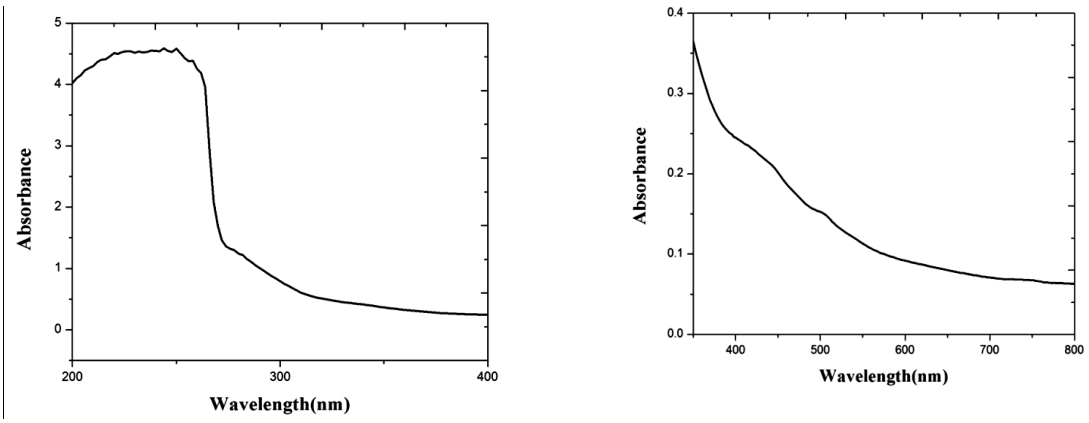

(b) (c)

Fig. 4. 4b, c. Electronic spectrum of Cu(II) complex 3

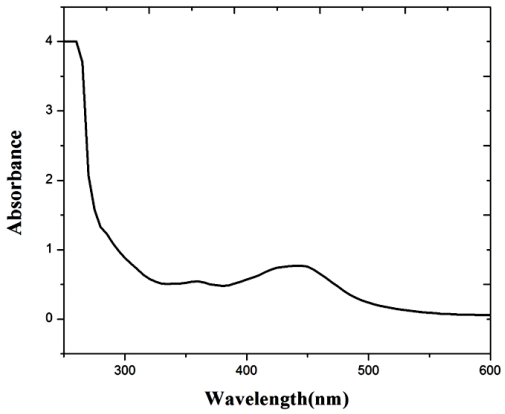

Fig. 4. 4d. Electronic spectrum of Cu(II) complex 4

The two Ni(II) complexes **5** and **6** (Fig. 4. 4e and f) possess a square planar geometry with diamagnetic nature that is reflected by the electronic spectrum. It

shows four absorption bands at 245, 395, 440, 500 and 240, 380, 435, 520 nm for **5** and **6** respectively. The first two transitions may be assigned to an LMCT transition, usually observed in metal Schiff base complexes containing "phenalato to M" charge transfer and the transition around 400 nm is due to $^1A_{1g} \rightarrow {}^1E_g$ transition. The transition at 500 and 520 nm is assigned to $^1A_{1g} \rightarrow {}^1A_{2g}$ which is a characteristic of square planar geometry. These transitions as well as a measured value of the magnetic moment (μ_{eff}= 0) prove its square planar geometry. Diamagnetism is a consequence of eight electrons being paired in the four low lying d-orbitals are often so close together in energy that individual transitions from there to the upper d_{x2-y2} orbital cannot be clearly distinguished resulting in a single absorption.

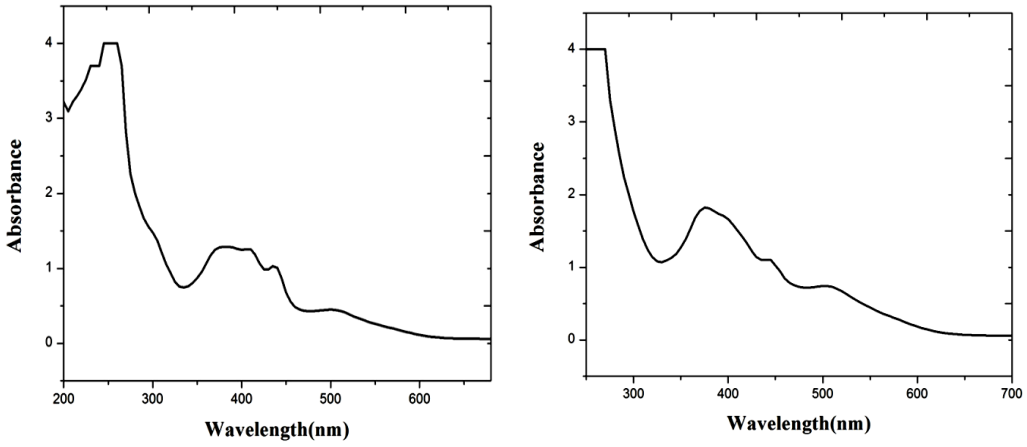

(e) **(f)**

Fig. 4. 4e and f. Electronic spectrum of Ni(II) complexes

The Co(II) complexes **7** and **8** (`Figs. 4. 4g-4h) show a shoulder like absorption peak at 228–290 nm region, which is assigned to the charge-transfer transition from the filled pπ orbital of the phenolic oxygen atoms to vacant d orbital of the metal. The complexes exhibited an absorption band at 382-386 nm, for d–d transition corresponding to $^4T_{1g}(F) \rightarrow {}^4T_{1g}(P)$ transition, suggesting an octahedral geometry. It has a magnetic moment of 5.18 BM indicating a high spin octahedral structure for the complex[24, 25].

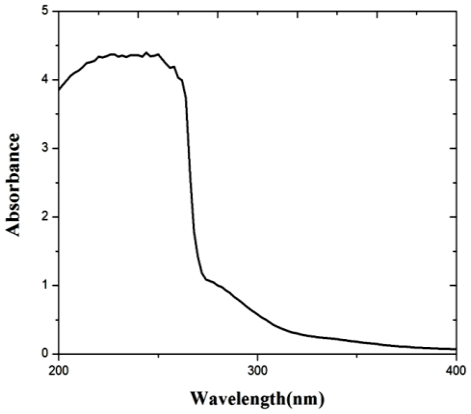

(g)

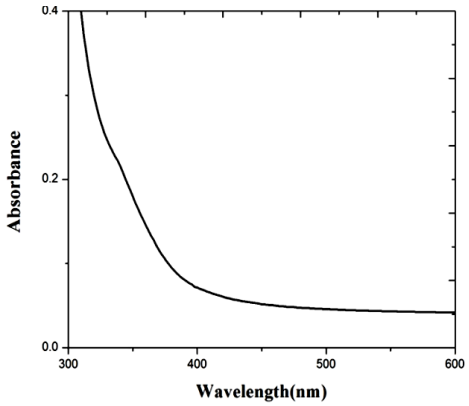

(h)

Fig. 4. 4g and h. Electronic spectrum of Co(II) complex 7

Table 4. 6. Electronic spectral details of the ligand and the complexes in nm

Compounds	UV spectral bands	Assignments
L^1	256, 310	$\pi\rightarrow\pi^*$, $n\rightarrow\pi^*$
L^2	258, 295	$\pi\rightarrow\pi^*$, $n\rightarrow\pi^*$
$[Cu(L^1)(ONO_2)]$	250,286,356, 448,513	Charge transfer, $^2B_{1g}\rightarrow{}^2A_{1g}$, $^2B_{1g}\rightarrow{}^2B_{2g}$
$[Cu(L^2)(ONO_2)]$	240, 355, 440,512	Charge transfer, $^2B_{1g}\rightarrow{}^2A_{1g}$, $^2B_{1g}\rightarrow{}^2B_{2g}$
$[Ni(L^1)(ONO_2)]$	245,305,395 440, 500	Charge transfer $^1A_{1g}\rightarrow{}^1E_g$, $^1A_{1g}\rightarrow{}^1A_{2g}$
$[Ni(L^2)(ONO_2)]$	240, 380, 435, 520	Charge transfer $^1A_{1g}\rightarrow{}^1E_g$, $^1A_{1g}\rightarrow{}^1A_{2g}$
$[Co(L^1)_2]$	228,290, 382.	Charge transfer $^4T_{1g}\rightarrow{}^4T_{1g}$.
$[Co(L^2)_2]$	234, 288, 386.	Charge transfer $^4T_{1g}\rightarrow{}^4T_{1g}$.

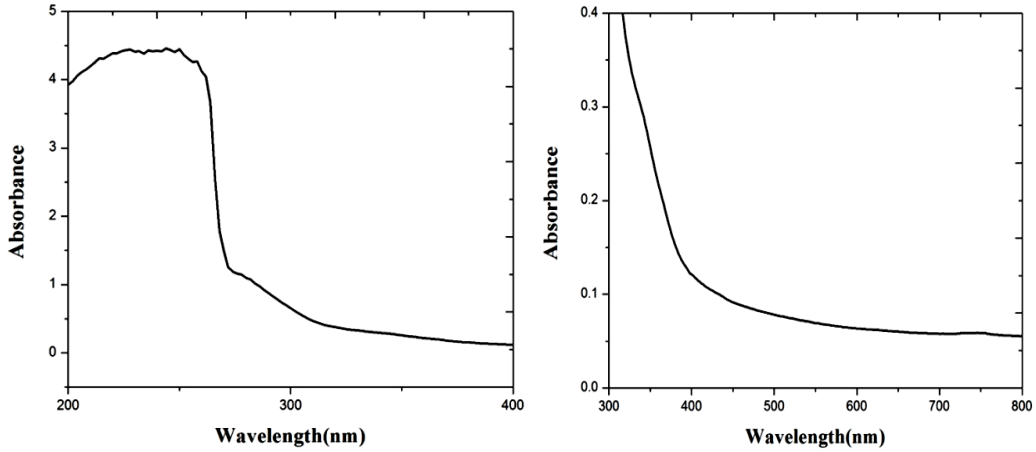

(h) **(i)**

Fig. 4. 4i and j. Electronic spectrum of Co(II) complex 8.

4.5.4. NMR Spectra

For studying the structure of the synthesized coordination compounds the ^{1}H-NMR spectra of coordination compounds and non-coordinated organic ligand have been studied and compared, because they can be used to characterize the position of the hydrogen atoms in the molecules of substances, as well as their number.

The proton NMR spectra of the Schiff bases almost show same chemical shift values except the aromatic protons which are slightly deshielded towards higher δ values. This is due to the presence of the electronegative bromo substituent. The ^{1}H-NMR spectra of compounds **1** (Figs. 4.5a and b) revealed a multiplet around 6.76-8.15 ppm for aromatic protons, peak at δ7.86 ppm is attributed to –CH=N protons. The peak at δ 4.54 and δ 8.11 ppm correspond to the –OH and –NH in the pyrimidine ring respectively. The peak at δ 11.57 ppm is due to the amino group in the ligand. The peak at 2.90 ppm is due to the solvent DMSO. The dimethylformamide present in the ligand shows peaks at δ 13.179 ppm due to the aldehydic proton and methyl protons at δ 3.48 ppm. The spectrum of **2** is similar with that of **1** with slight shift in the peaks. The spectrum of the complexes **5** and **6** (Fig. 4.6a and b) differs from that of the free ligand in the following aspects

1. The disappearance of the signal due the phenolic –OH group at δ 4.54 ppm is attributed to its involvement of it in co-ordinating to the nickel cation and the appearance of –OH group peak at δ 14.3 proves the enolisation of –C=O group.

2. The displacement of band -NH_2 groups in the ^{1}H NMR spectra of the studied coordination compounds in the region of strong field compared with the absorption bands of the same groups in ^{1}H NMR spectrum of non-coordinated ligand is noted, which testifies the co-ordination of the amino group to the metal. The bond between -NH_2 group and the central metal ion in complexes is formed without the replacement of hydrogen atoms as the number of protons of free ligand and organic part of the synthesized coordination compounds is the same.
3. The other signals are slightly deshielded due to the complexation and the solvent DMF is absent which is confirmed from the disappearance of its peak.

4.5.5. Thermogravimetric analysis of the complexes

The thermal behavior of the synthesized complexes has been studied to establish different decomposition process and to confirm the proposed stoichiometry. The results of such analysis have been summarized in Table 4.7 indicating a good correlation between calculated and found weight loss values. The thermograms of all the complexes are given in Figs. 4.7a-f respectively.

4.5.5.1. Cu(II) complexes 3 and 4

The thermal dehydration and denitration of the Cu(II) complexes in the first stage accounts for a mass loss of 5.5 % and 15.6 % for **3** and **4** respectively, leaving behind the non-hydrated complex which takes place between 40-310°C. The maximum rate of mass loss is indicated by the DTG peak at 73.41°C and 102.34°C for the lattice water and 199.01 and 204.24°C for the co-ordinated nitrate ion as nitric acid.

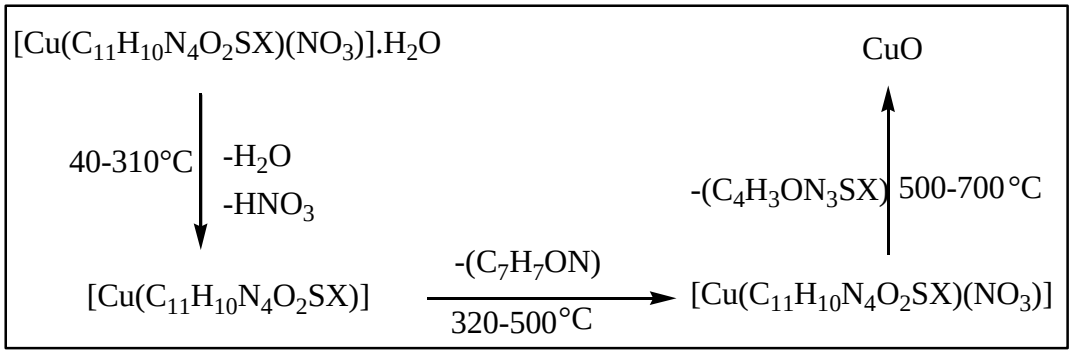

The remaining complex begins to decompose from the range 320-700°C with DTG peak observed at 367.74 and 510.13°C for **3** and 282.68 and 350.00°C for **4** with a total mass loss of 62.8 and 54.5% respectively. The overall mass loss was 86.41 and 83.66% respectively and it was compared with the theoretical mass value. The end

product estimated as CuO and the observed mass and the calculated mass were overall equal. As a result the observed product was in good agreement with the metal oxide.

4.5.5.2. Ni(II) complexes 5 and 6

The decomposition pattern of the Ni(II) complexes are similar to Cu(II) complexes since they are isostructural. The temperature range with the mass loss percentage is given in Table 4.7. The end product after all the decomposition patterns is NiO.

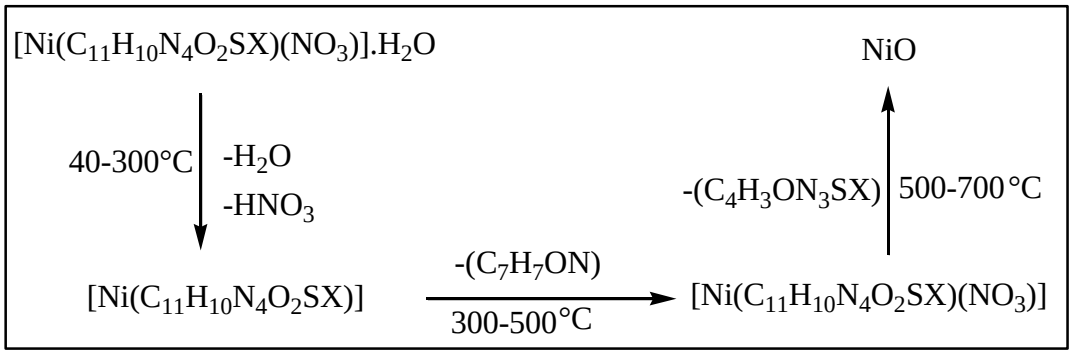

4.5.5.3. Co(II) complexes 7 and 8

The decomposition pattern of Co(II) complex is different from Cu(II) and Ni(II) complexes. The two lattice solvent DMF molecules are lost in the temperature range 140-300°C. After the loss of guest solvent molecules, the network began to decompose with the continuous weight loss upto 500°C with a DTG peak at 108.48 and 304.31°C for **7** and 143.37 and 308.22°C for **8** respectively. After the decomposition of all the organic part of the ligand the residue left behind is the CoO[26, 27].

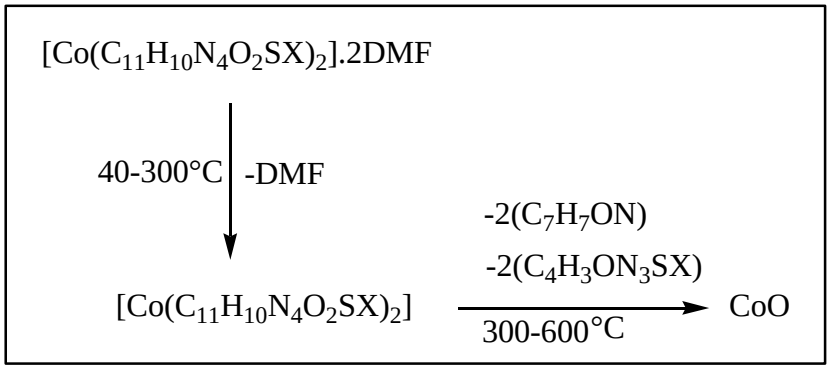

4.5.6. Mass spectral analysis

The mass spectrum of the complexes is in good agreement with the proposed molecular structure and the mass spectrums of the complexes **3** and **8** are shown in Fig. 4.8a to f respectively. The molecular ion peak [M^+] appeared at m/z= 406.9,

485.8, 402.0, 480.9, 731.7, 889.5 confirming the stoichiometry of the complexes 3-8 respectively.

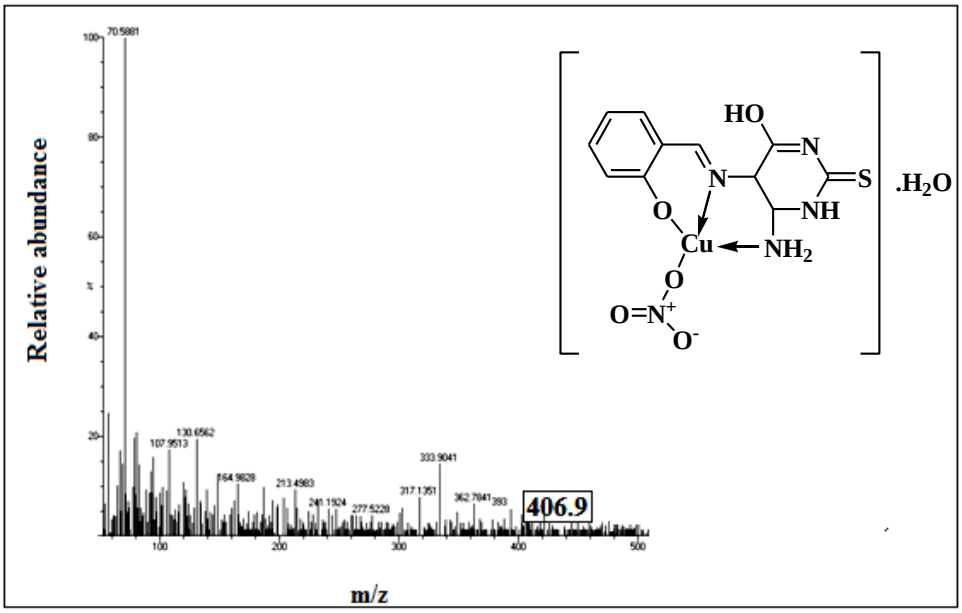

Fig. 4.8a. Mass spectrum of Cu(II) complex 3

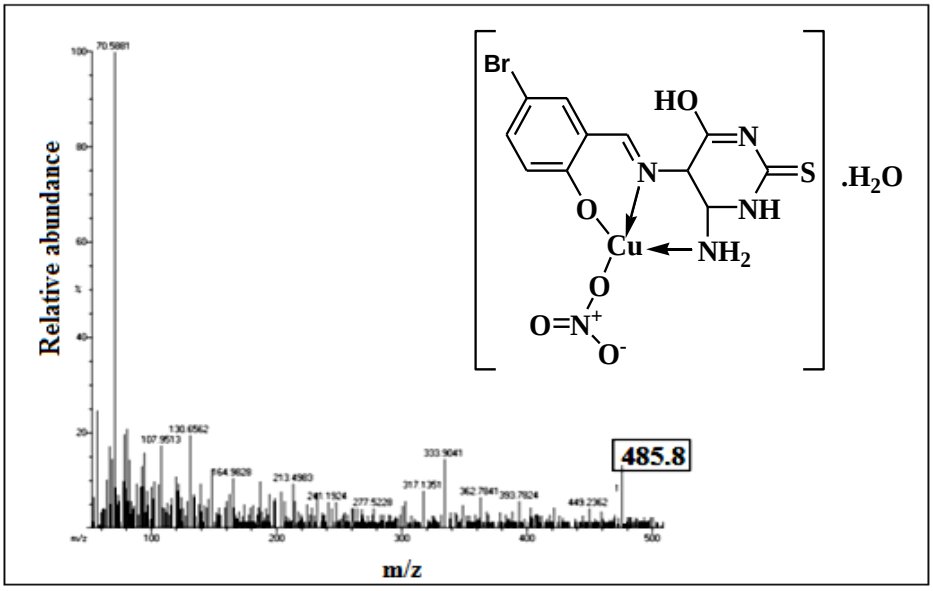

Fig. 4.8b. Mass spectrum of Cu(II) complex 4

4.5.7. ESR Spectral data of the Cu(II) complexes

Based on hyperfine and super hyperfine structures, the ESR spectrum of metal complexes (Fig.4.9) provide information about the environment of the metal ion within the complexes, *i.e.*, the geometry and nature of the legating sites of the Schiff base and the metal. The ESR spectra of the Cu(II) complexes **3** and **4** were recorded at room temperature. The shift of the signal in the low-field region to a slightly lower value indicates stronger metal–ligand bonding. The Cu(II) chelates **3** and **4** showed two peaks, one in the low field region and the other in the high field region, from which g_{ll} and $g_{\perp}$ were calculated (Table 4.8).

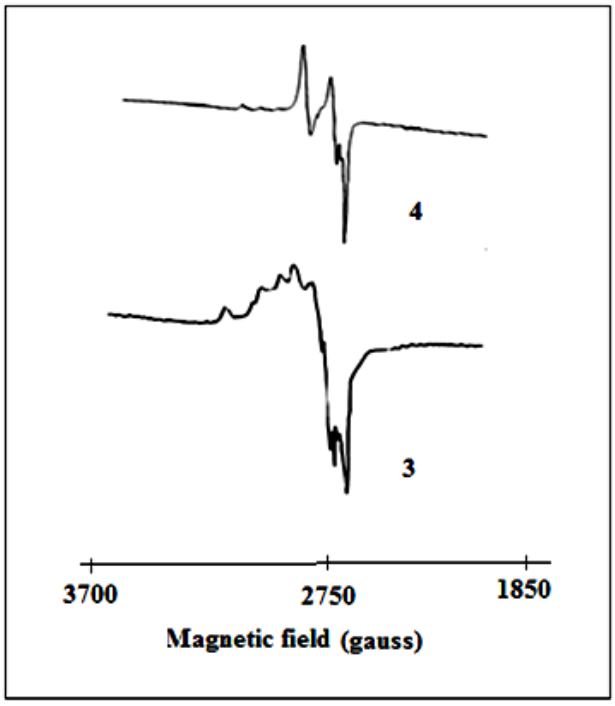

Fig. 4. 9. ESR Spectrum of 3 and 4

The gll values (<2.3) indicate covalent character of the metal–ligand bonds. The covalent nature of the metal–ligand bond in the complex is further supported by the g_{eff} value, which was lesser than 2.0023. The value $g_{ll} > g_{\perp}$ is well consistent with a primarily d_{x2-y2} ground state. The d_{x2-y2} ground state is characteristic of square planar, square pyramidal, tetrahedral or octahedral stereochemistry. The gll/All value can be used to determine the stereochemistry of the copper (II) complex. The range reported for square planar complexes is 105– 135 cm^{-1} and for tetrahedrally distorted complexes 150–250 cm^{-1}. The g_{ll}/A_{ll} value is in the range of 132-133 cm^{-1} for these complexes suggesting square planar geometry[28].

Table 4.8. ESR spectral parameters

g_{11}	$g_{\perp}$	g_{av}	A_{11} $x10^{-4}$ cm^{-1}	$A_{\perp}$ $x10^{-4}$ cm^{-1}	g_{11}/A_{11} cm	G	α^2	β^2
2.18	2.03	2.11	165	59	132	4.67	0.50	1.12
2.23	2.09	2.17	167	69	133	4.33	1.27	0.78

4.5.8. EDX Spectral details of the complexes

The chemical analysis results by EDX for the formed complexes show a homogenous distribution in between metal ions and chelating agent. The peaks of EDX profile of Cu(II), Co(II) and Ni(II) complexes (Figs.4.10-12) refer to all elements which constitute the molecules of Schiff base complexes confirming the proposed structures. The weight percentage of the metal, carbon and nitrogen were calculated and compared with the values from analytical data and EDX (Tables 4.9-4.11). The values are in good agreement with each other and hence the structures of the complexes are tentatively proposed as shown in Figs.4.13a-c respectively.

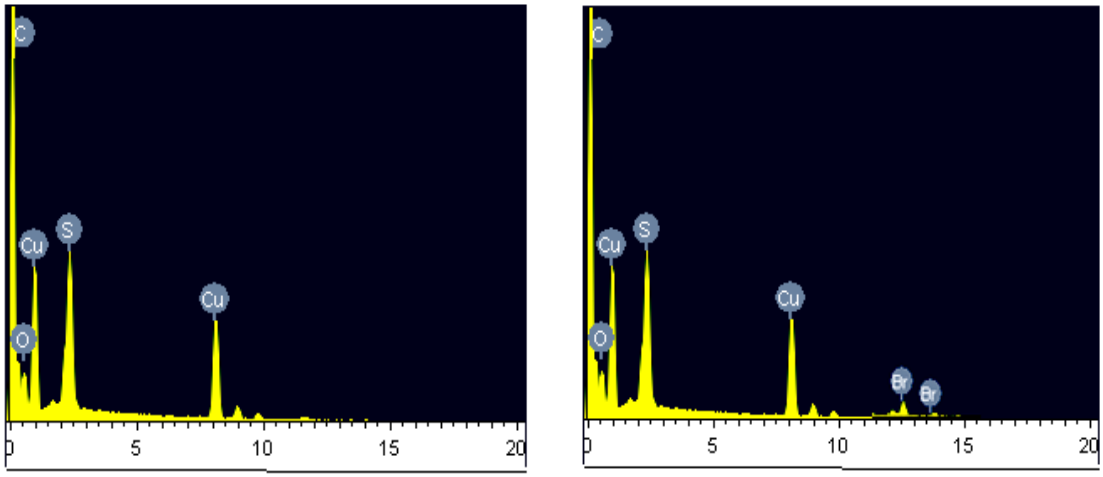

Fig. 4.10. EDAX spectrum of Cu(II) complexes 3 and 4

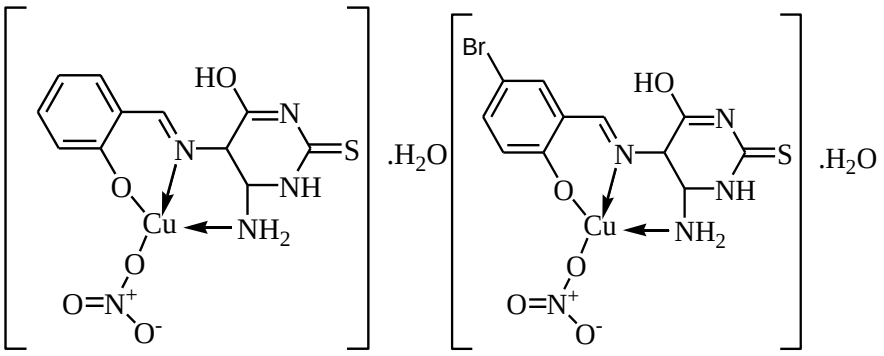

Fig. 4.13a. Proposed structure of Cu(II) complexes

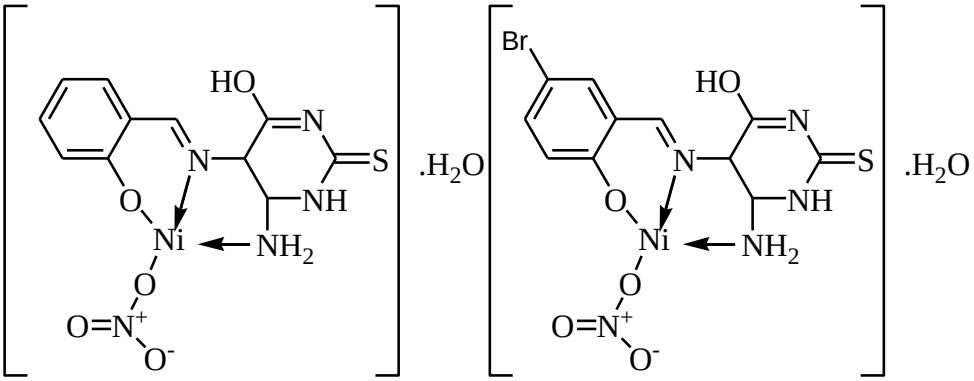

Fig. 4.13b. Proposed structure of Ni(II) complexes

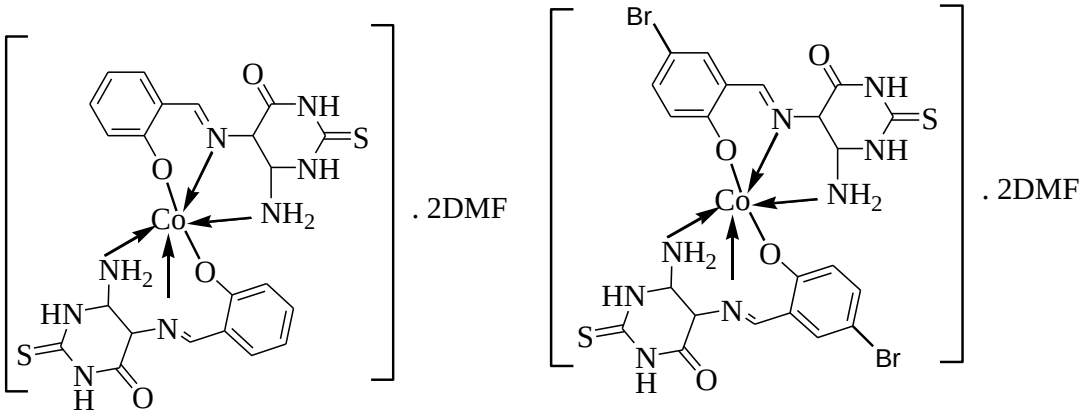

Fig. 4.13c.Proposed structure of Co(II) complexes

4.5.9. Theoretical structure of the complexes

The molecular structures of the complexes were investigated theoretically using the Gaussian 09 program by the UB3LYP methods with 6-31G(d,p) basis sets. Randomly selected geometric parameters (bond length and bond angles) were theoretically calculated for the Cu(II) and Ni(II) complexes and listed in Table 4.12 and 4.13. The optimized geometry of the complexes **3** to **6** are given in Figs. 4.14a and b respectively.

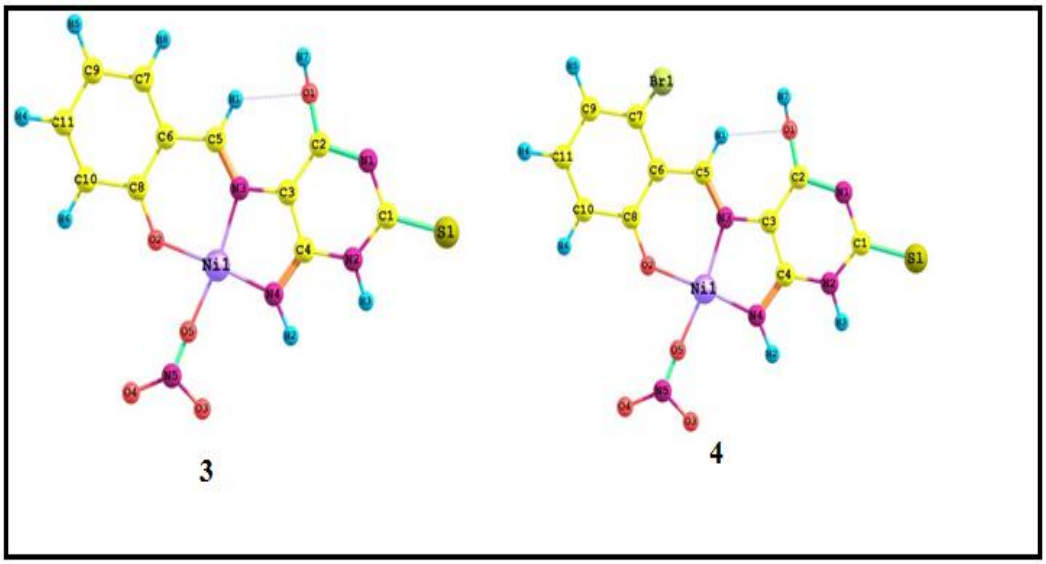

Fig. 4.14a. Optimized geometry of Ni(II) complexes

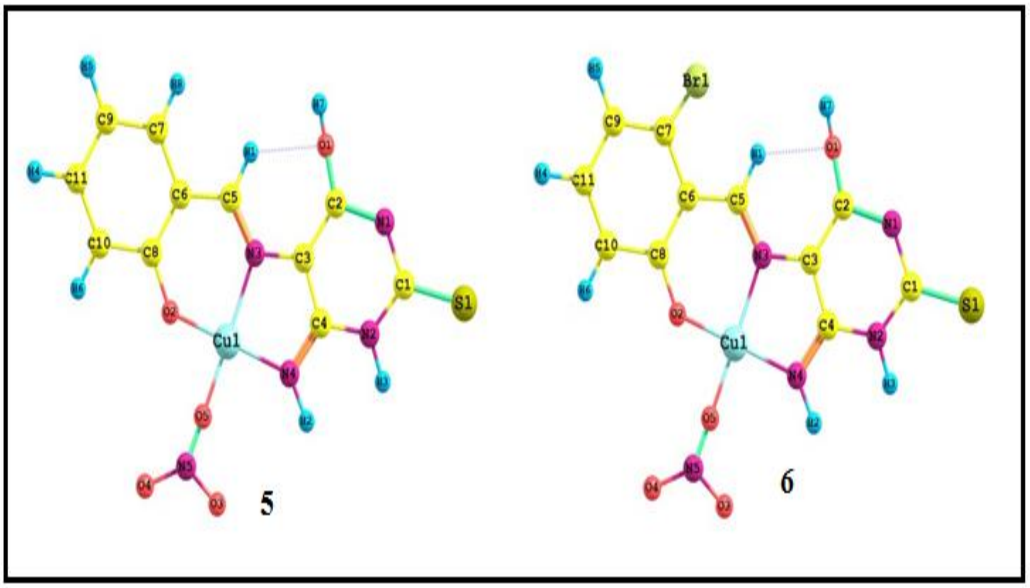

Fig. 4.14b. Optimized geometry of Cu(II) complexes

4.5.10. HOMO-LUMO Calculations

Theoretical analysis of the electronic structure of complexes can establish the relationships between molecular structure and electronic properties. Theoretical studies on the electronic structures of π-conjugated complexes have given great contributions to the rationalization of the properties of known materials and to the prediction of the yet unknown ones. In this context, quantum chemical methods have been increasingly applied to predict the band gap of metal complexes and comparing them with the ligand. This work will further elucidate geometric and electronic properties with the aim to prove the relationship between molecular structure and electronic properties, and driving towards the next synthesis of compounds which are active materials in optoelectronic. The quantum chemical investigation has been performed to gain knowledge on the optical and electronic properties of pyrimidine derivatives. The theoretical knowledge of the HOMO and LUMO energy levels of the components forms the basis for the study of organic solar cells. The HOMO, LUMO and gap energy of the studied compounds have been calculated and reported. Their properties suggest they are good candidates for optoelectronic applications.

The highest occupied molecular orbital (HOMO) and lowest unoccupied molecular orbital (LUMO) are the most important orbitals in a molecule. HOMO, which can be thought as the outer orbital containing electrons, tend to give these electrons as an electron donor and hence the ionization potential is directly related to the energy of the HOMO. On the other hand LUMO can accept electrons and the LUMO energy is directly related to electron affinity.

Two important molecular orbitals (MO) were examined for the ligand (Fig.4.15) and the complexes (Fig. 4.16 and 4.17), the highest occupied molecular orbital (HOMO) and the lowest unoccupied molecular orbital (LUMO). For understanding various aspects of pharmacological sciences including drug design and the possible ecotoxicological characteristics of the drug molecules, several new chemical reactivity descriptors have been proposed. Conceptual DFT based descriptors have helped in many ways to understand the structure of molecules and their reactivity by calculating the chemical potential, global hardness and electrophilicity. Using HOMO and LUMO orbital energies, the ionization energy and electron affinity can be expressed as: $I = - E_{HOMO}$, $A=-E_{LUMO}$, $\eta = (^{-}E_{HOMO}+E_{LUMO})/2$ and $\chi =1/2(E_{HOMO} + E_{LUMO})$. Parr et al. proposed the global electrophilicity power of a

ligand S = l/2 η. This index measures the stabilization in energy when the system acquires an additional electronic charge from the environment. Electrophilicity encompasses both the ability of an electrophile to acquire additional electronic charge and the resistance of the system to exchange electronic charge with the environment. It contains information about both electron transfer (chemical potential) and stability (hardness) and is a better descriptor of global chemical reactivity. It is seen that the chemical potential of the title compound is negative and it means that the compound is stable. They do not decompose spontaneously into the elements they are made up of. The hardness signifies the resistance toward the deformation of electron cloud of chemical systems under small perturbation encountered during the chemical process. The principle of hardness works in Chemistry and Physics but it is not physically observable. Soft systems are large and highly polarizable, while hard systems are relatively small and much less polarizable[29, 30]. The calculated ionization potential, electron affinity, hardness and softness are tabulated in Table 4.14.

Table 4.14. The calculated frontier orbital energies, electronegativity, hardness and softness of ligand using UB3LYP/6-31G (d) level

	1	**2**	**3**	**4**	**5**	**6**
E_{HOMO}(eV)	-5.2923	-5.5919	-6.8249	-6.9718	-5.9985	-6.2042
E_{LUMO}(eV)	-1.4260	-1.8041	-6.4317	-6.6671	-5.2232	-5.4025
I (eV)	5.2923	5.5919	6.8249	6.9718	5.9985	6.2042
A (eV)	1.4260	1.8041	6.4317	6.6671	5.2232	5.4025
χ (eV)	3.3591	3.6980	6.6283	6.8194	5.6108	5.8033
η (eV)	1.9331	1.8939	0.3393	0.1523	0.3876	0.4008
S(eV^{-1})	0.2586	0.2640	1.4736	3.2829	1.2899	1.2475

Atomic charge distributions on donor-acceptor atoms of the complexes and donor atoms of the free ligands were calculated at B3LYP level of theory. Charge distributions between donor atom of ligands and acceptor atoms of complexes were evaluated by natural population analysis in gas phase. The charge distribution results are listed in Table 4.14. Comparing the atomic charges in Table 4.15, it is evident that the atomic charge presented by the electronegative atoms in ligand decreases after complex formation while the electron density of the metal ions increased. After

complexation, the charge on the metal has been reduced indicating that ligand transfers their negative charges to metal ions during formation of the complexes.

Table 4.15. Atomic charges from the natural population analysis

Atom	1	3	5	2	4	6
M	-	1.020	0.877	-	1.027	0.987
N(1)	-0.711	-0.691	-0.689	-0.713	-0.687	-0.682
N(2)	-0.672	-0.676	-0.699	-0.685	-0.665	-0.668
N(3)	-0.711	-0.724	-0.737	-0.704	-0.712	-0.745
N(4)	-0.552	-0.723	-0.689	-0.534	-0.723	-0.634
N(5)	-	0.359	0.372	-	0.358	0.372
S(1)	-0.448	-0.004	-0.004	-0.434	-0.004	-0.004
O(1)	-0.675	-0.446	-0.442	-0.673	-0.446	-0.442
O(5)	-0.598	-0.606	-0.601	-0.589	-0.612	-0.601
O(2)	-	-0.342	-0.278	-	-0.341	-0.276

Ayhan *et al.,* synthesized some of the 2-oxopyrimidin-1(2*H*)-yl-amide derivatives and studied their molecular properties using DFT calculations and the E_{HOMO} values range from -6.44eV to -6.56eV. The frontier orbital energies for the sulphur containing molecules were found low[31]. Hatem *et al.,* synthesized new derivatives of Thieno[3,2-*d*]pyrimidine derivatives and the inspection of HOMO-LUMO energy gap (0.267eV to 0.292eV) indicates that these compounds are more liable to electron transfer reactions[32]. Durgadevi *et al.,* synthesized and characterized 5-(3-bromo-4-fluorobenzylidenepyrimidine-2,4,6(*1H,3H,5H*)-trione and molecular investigation was done and the calculated HOMO-LUMO gap is 3.99eV[33]. Azantha *et al.,* synthesized some of the 2-aminopyrimidine derivatives and their DFT calculations show that the HOMO-LUMO energy gap is in the range from 0.19 to 0.21eV. Compared to these results in the literature, these pyrimidine ligands showed a low HOMO-LUMO energy gap and also not much of the reports of pyrimidine derivatives and its complexes and their HOMO LUMO calculations has been reported. So these derivatives will definitely are of much important for the future researchers to explore the molecular properties of pyrimidine derivatives and its complexes[34].

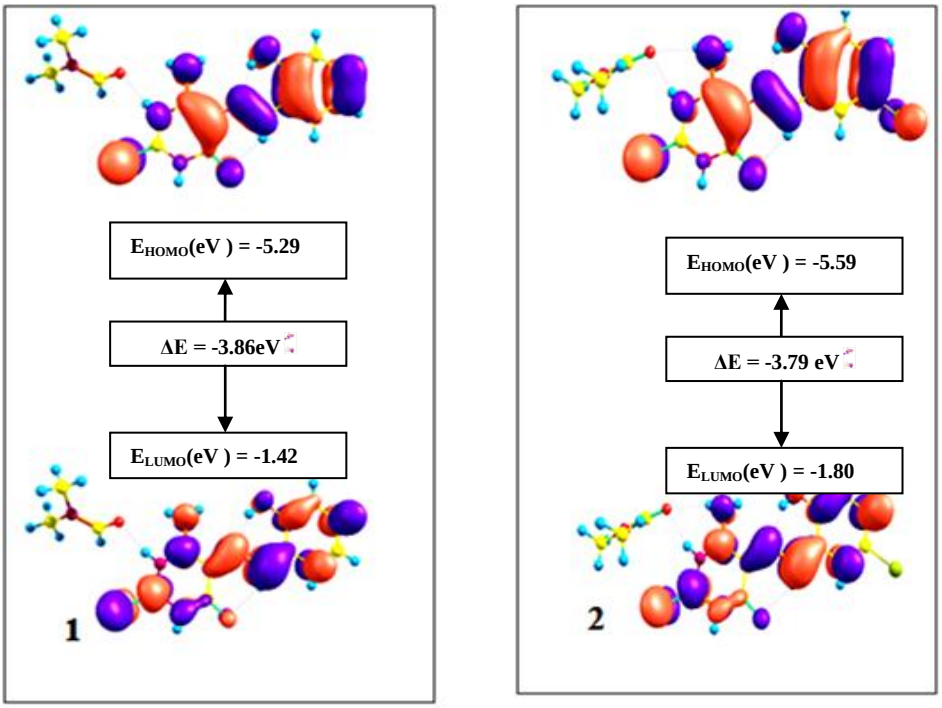

Fig. 4.15.The ground state isodensity surface plots for the frontier molecular orbitals for 1 and 2

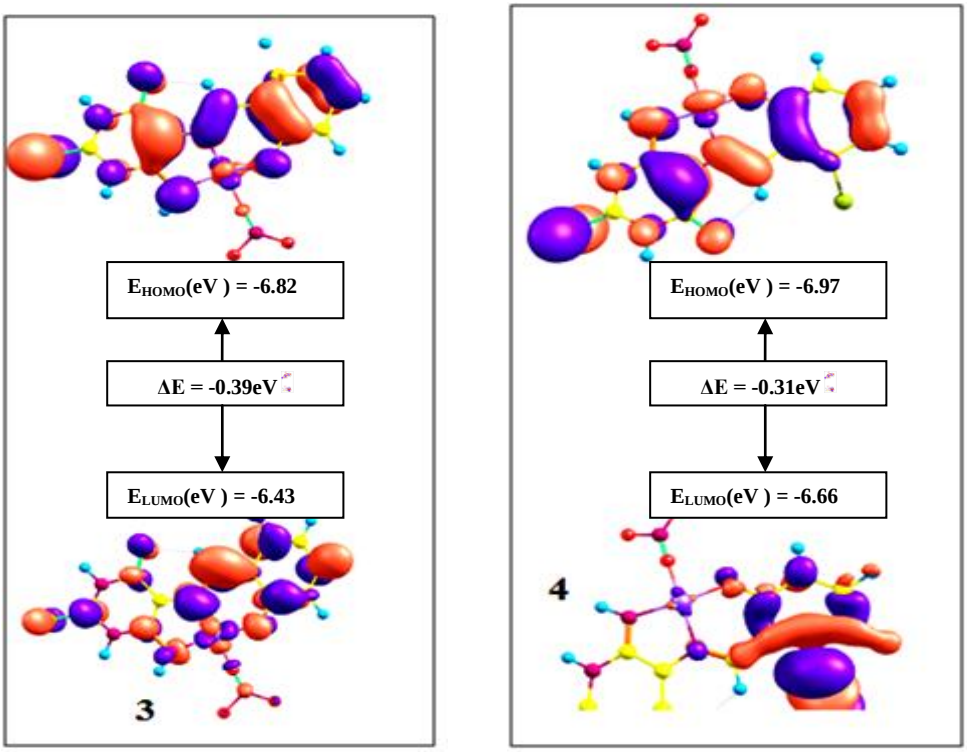

Fig. 4.16.The ground state isodensity surface plots for the frontier molecular orbitals for 3 and 4

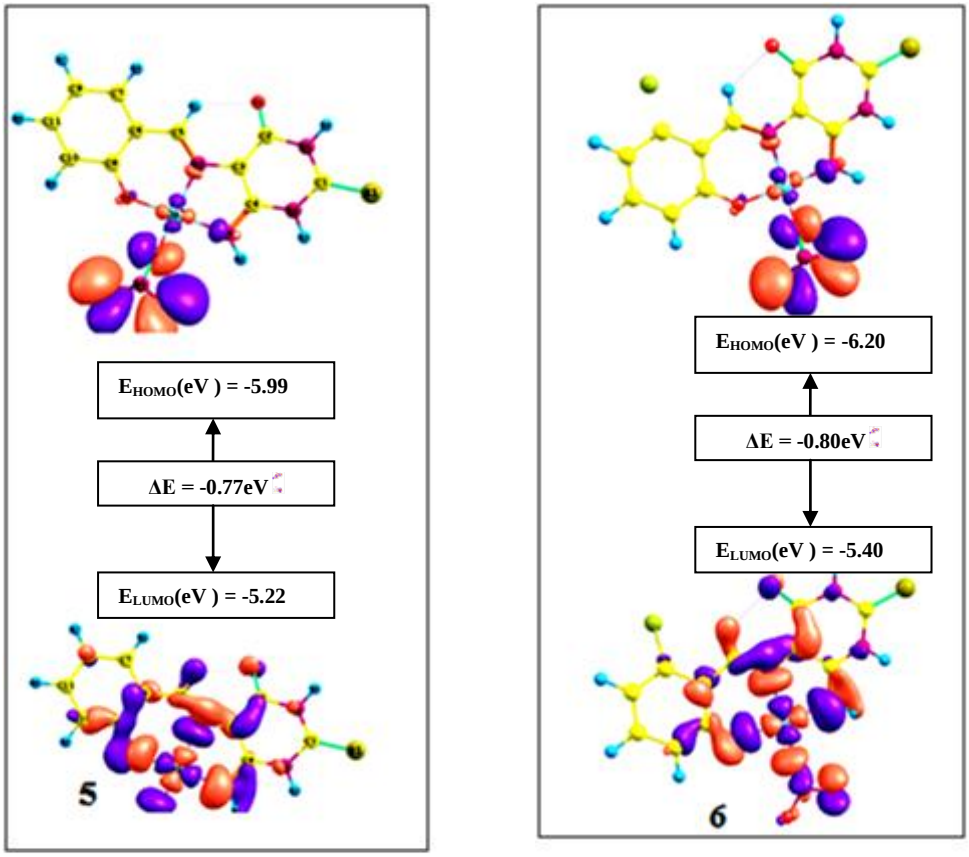

Fig. 4.17.The ground state isodensity surface plots for the frontier molecular orbitals for 5 and 6

4.6. Pharmacology

4.6.1. Antimicrobial studies

In-vitro microbial activity against certain bacterial and fungal species was screened for the free ligands and the metal complexes using well diffusion method. The antimicrobial activities of the newly synthesized ligands were tested against the pathogens *viz., Pseudomonas aeroginosa, Escherchia coli, Thiobacillus thidurance, Serratia marcescens, Acinetobater baumauii, Aspergillus niger* and *Candida albicans.* The results illustrated in (Figs. 4.18a, b) revealed that the tested compounds had a good antibacterial activity than the standard antibiotics. However, in most of the cases they possessed 50% of the activity of the standards. Compound **2** showed a greater activity than **1** on almost all the pathogens. Compound **2** showed pronounced activity against *Candida albicans, Escherchia coli, Thiobacillus thidurance* and *Serratia marcescens*.. Compound **1** showed good activity against *Aspergillus niger* and a moderate activity against all the other organisms under study. The standards used for

the antibacterial and antifungal activity were *Ciprofloxacin* and *Fluconazole* respectively[35].

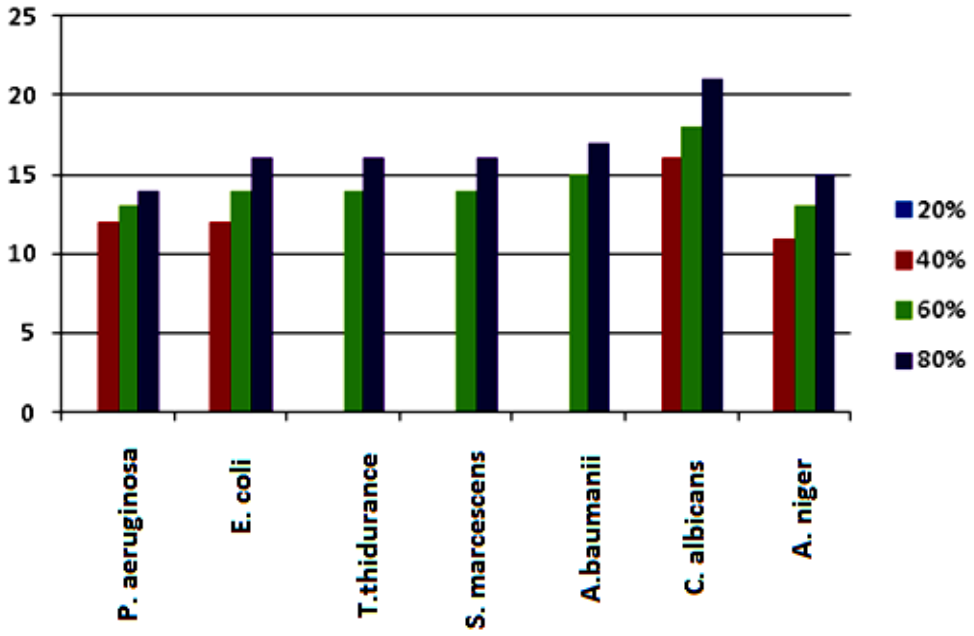

Fig. 4.18a. Antimicrobial activity of ligand 1

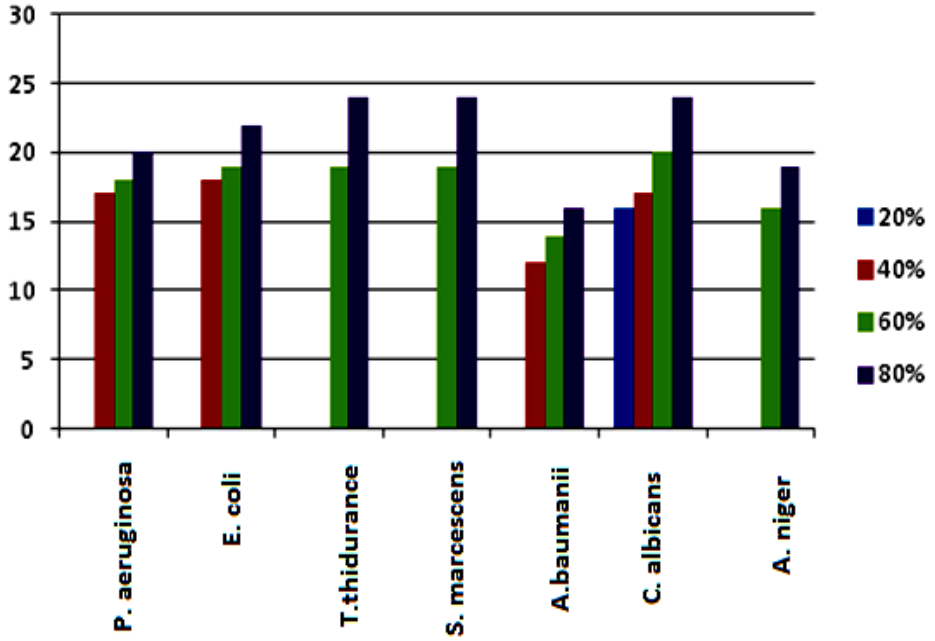

Fig. 4.18b. Antimicrobial activity of ligand 2

Table 4.17. MIC values for 1 and 2

S.No	Organisms	1000 µg/ml	500 µg/ml	250 µg/ml	125 µg/ml	62.5 µg/ml	31.25 µg/ml	15.625 µg/ml
Schiff base 1								
1.	*T.thidurance*	-	-	+	+	+	+	+
2.	*E.coli*	-	-	-	-	+	+	+
3.	*C. albicans*	-	-	-	+	+	+	+
Schiff base 2								
1.	*T.thidurance*	-	-	-	+	+	+	+
2	*E. coli*	-	-	-	-	+	+	+
3.	*C. albicans*	-	-	-	+	+	+	+

The minimum inhibitory concentration of **1** and **2** (Table 4.17) *against T. thidurance, E. coli* and *C. albicans* are 500, 125, 250 µg/ml and 250, 125 and 250 µg/ml respectively.

The anti-microbial activity for the complexes has been checked for the three species against *T. thidurance*, *E. coli* and *C. albicans* and found to be greater than the free ligands. This can be attributed to the Tweedy's chelation theory according to which chelation reduces the polarity of the metal atom mainly because of the potential sharing of its positive charge with the donor group and possible π-electron delocalization over the whole ring. This increases the lipophilic character of the metal chelate, favouring its permeation through the lipid layers of the bacterial membranes. Furthermore, the mode of action of the compounds may involve hydrogen bonding *via.,* the >C=N group with active centers of cell constituents resulting in the interference with normal cell process. The activities of the complexes have been compared with the activity of the standard bacteriocide (Ciprofloxacin) and fungicide (Fluconazole) and it has been found that the complexes show better activity. Table 4.18 shows the minimum inhibitory concentration of the complexes *against T. thidurance, E. coli* and *C. albicans*.

4.6.2. In-vitro anticancer activity

Of the various human diseases, cancer is the most intractable disease for which no practical and generally effective drugs or methods of control are available. Therefore, the identification of novel, potent, selective, and less toxic anticancer agents remains one of the most pressing problems. Cancer is a complex disease that is normally associated with a wide range of escalating effects both at the molecular and cellular levels. The ligands **1** and **2** synthesized were evaluated for their cytotoxicity against human breast cancer cell line MCF-7 by means of MTT assay that measured

mitochondrial dehydrogenase activity as an indication of cell viability. The results were analysed by means of cell viability curves and expressed in IC_{50} values in the studied concentration range of 0.1 to 100 μM. The activity of the compounds that corresponds to the inhibition of cancer cell growth at a maximum level is shown in Fig. 4.19.

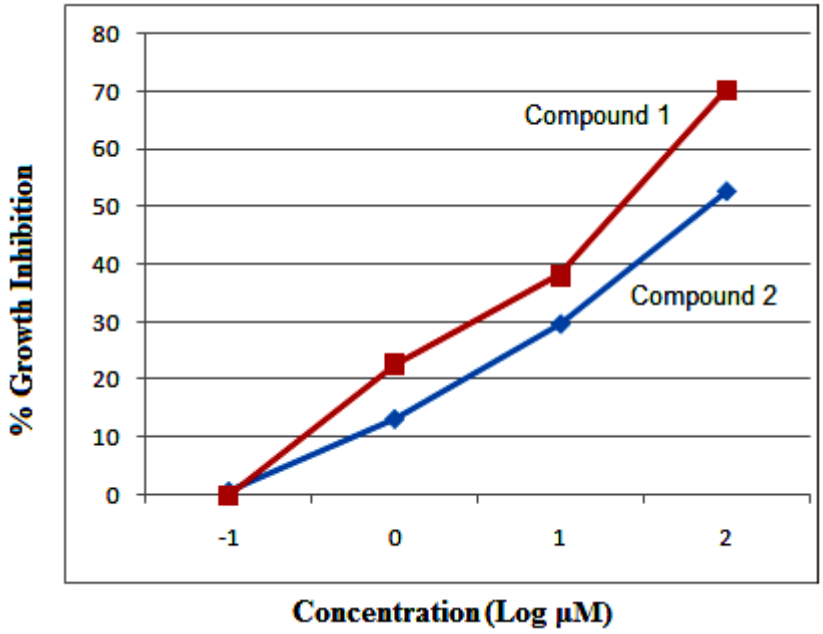

Fig. 4.19. Percentage growth inhibition of MCF-7 cell line as a function of concentration of the compounds **1** and **2**

The results of MTT assay revealed that the compound **2** possessed higher cytotoxic effect than **1**. The presence of bromo substituent in **2** has enhanced the cytoxicity compared to ligand **1.** The IC_{50} values of **1** and **2** were 83.24 μM and 54.22 μM respectively. The data obtained for our compounds showed cytotoxicity with short incubation period (48 h) and hence the data are highly significant[36].

4.6.3. DNA Binding Study

4.6.3.1. Absorption spectral measurements

Electronic absorption spectroscopy is an effective method to examine the binding mode of DNA with metal complexes. In general, hypochromism and red-shift are associated with the binding of the complex to the helix by an intercalative mode involving strong stacking interaction of the aromatic chromophore of the complex between the DNA base pairs. It is generally accepted that the DNA is the primarily pharmacological target of many metal based antitumor agents. The binding activities of DNA-metal complexes have been very much important to identify the mechanism of effective metal based chemotherapeutic drugs. Monitoring the effect of adding

increasing amounts of DNA on the absorption spectrum of metal complexes and thereby calculating the intrinsic binding constants will help in finding the type of binding of the metal complexes with DNA[37,38].

Many compounds exert anticancer effect through binding to DNA, thereby changing the replication of DNA and inhibiting the growth of the tumor cells, which is the basis for designing new and efficient anticancer drugs. Depending on their mode and affinity of binding the effectiveness of the compounds as DNA intercalators and therefore the binding of the compounds to DNA are considered to be highly important in the development of new anticancer drugs.

Electronic absorption and fluorescence spectroscopy are the effective methods to examine the binding modes of the Schiff bases with DNA. Compounds binding through intercalation usually results in hypochromism with or without small red or blue shift, since the intercalative mode involves a strong interaction between the planar aromatic chromophores and the base pairs of DNA. On the other hand, electrostatic binding is accompanied by a hyperchromic shift of absorption. The results of absorption spectra of the compounds **1** and **2** in the absence and presence of CT-DNA are shown in Figs. 4.20 respectively. With a fixed concentration of the compounds, the UV–visible spectra were recorded with the increasing amount of DNA. As shown in the figure, the maximum absorption peak observed for DNA at 260 and 258 nm proportionally increased with the increasing concentration of ligands **1** and **2**. This hyperchromic shift indicates that the interaction of the ligands with DNA is through electrostatic binding[39].

A majority of reports indicate that the presence of labile ligand units play a vital role in the DNA-binding strategy of metal complexes. Effectiveness of the DNA binding depends on the nucleophilic nature of the labile ligand attached to the metal center and the nature of the metal ion itself. In the present complexes, the architecture of the ligand is such that it provides atleast one labile ligand *viz.*, pyrimidine moiety, which is responsible for the interaction of the compounds with N-7 of nucleotide, which leads to the perturbation of DNA structure, and hence inhibiting the replication. In the present investigation by following the changes in absorbance and shift in the wavelength as a function of added concentration of DNA, the binding of metal complexes (25μM) to CT-DNA in different concentrations (0-40 μM) has been characterized classically. The electronic spectra of the complexes **(3** to **8)** upon the addition of CT-DNA are shown in Figs. 4.20c-e respectively.

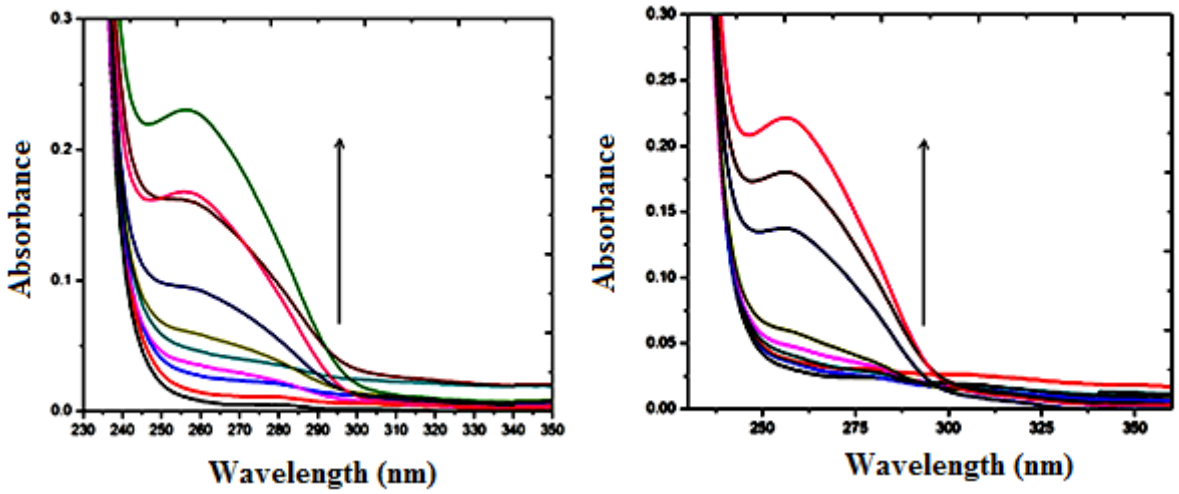

Fig. 4.20a. Absorption spectra of the ligands 1 and 2 in the presence and absence of CT-DNA. Conditions: [M] = 10µM, [DNA] = 0-60 µM. Arrow (↓) shows the absorbance changes upon increasing DNA concentration

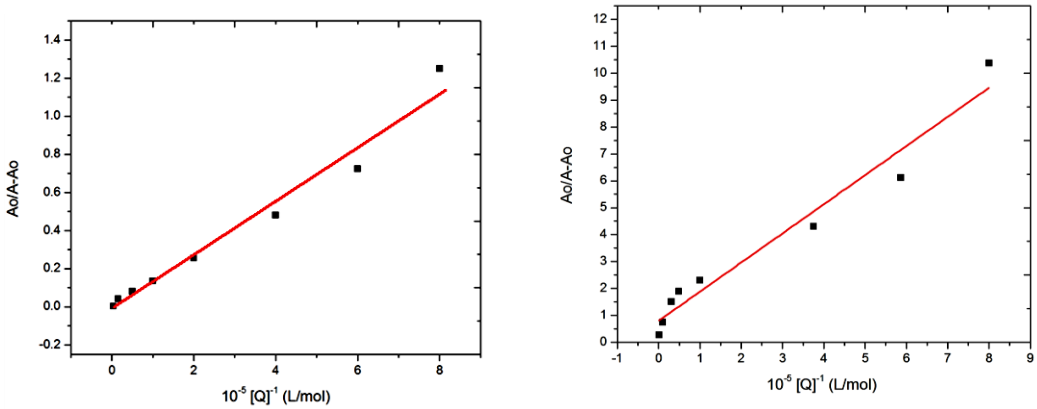

Fig.4.20b. Linear plot for the calculation of the intrinsic DNA binding constant, K_b for the ligands 1 and 2.

As already stated, the addition of the compounds (10^{-6} mol dm^{-3}) to CT-DNA resulted in a hyperchromic shift of the absorption band at 260 nm. The following equation can be utilized to calculate the binding constant (K) taking into account the variations in the absorption spectra of DNA binding to the Schiff bases and its complexes. Absorption titrations were performed by keeping the concentration of the complex constant(10µM) and by varying the concentration of CT-DNA from 0 to 60µM. The binding constant (K_b) for the complexes have been determined from the following equation.

$$\frac{[DNA]}{(\epsilon_A - \epsilon_F)} = \frac{[DNA]}{(\epsilon_B - \epsilon_F)} + \frac{1}{K_b(\epsilon_B - \epsilon_F)}$$

where ε_A, ε_B and ε_F correspond to the apparent, bound and free metal complex extinction coefficients respectively. A plot of [DNA] / (ε_A-ε_F) versus [DNA] gave a slope of $1/(\varepsilon_B-\varepsilon_F)$ and a Y intercept equal to $1/K_b(\varepsilon_B-\varepsilon_F)$, where K_b is the ratio of slope to the intercept yielding the binding constants, $K = 4.07 \times 10^3$ and 2.58×10^3 mol^{-1} dm^3 of **1** and **2** respectively.

The observation of hypochromism is indicative of intercalative mode of binding of DNA to the complexes along with the stabilization of the DNA double helix structure. On the other hand, the observation of hyperchromism is indicative of the breakage of the secondary structure of DNA. Hence the observation of hyperchromism with red shift for our complexes showed that that the new complexes interact with the secondary structure of CT-DNA by breaking its double helix structure. In order to compare quantitatively the binding strength of the complexes, the intrinsic binding constants (K_b) of them with the CT-DNA were determined from the above equation and the binding constants of the complexes **3** to **8** are 1.2 X 10^4 M^{-1}, 9.2 X 10^4 M^{-1}, 4.2 X 10^4 M^{-1}, 1.5 X 10^4 M^{-1}, 1.8 X 10^4 M^{-1} and 2.5 X 10^4 M^{-1} respectively. The K_b values of all the complexes are in the order of 10^4 M^{-1}. The linear plots for the calculation of binding constants are shown in Fig.4.20b and 4.20f-h for the ligands and the complexes respectively.

4.6.3.2. Fluorescence spectroscopic studies

In the absence of CT-DNA, Schiff base ligand (1 and 2) and complexes **3** to **8** emit strong luminescence in Tris–HCl buffer at ambient temperatures with a maxima appearing at 430-450 nm (excited at 280 nm). Upon addition of increasing concentration of CT-DNA to the fixed amount of complexes, there was enhancement of the emission intensity indicative of strong interaction of the complexes with CT-DNA. Although the emission enhancement could not be regarded as a criterion for binding mode, they are related to the extent to which the complex gets into the hydrophobic environment inside the DNA and avoid or reduce the accessibility of solvent molecules to complex. The enhancement of the emission intensity is largely due to the inaccessibility of the solvent water molecules to reach the hydrophobic environment inside the DNA helix and mobility of the complex was restricted at the binding site ultimately leading to decrease in vibrational mode of relaxation and thus higher emission intensity. Hydrophobic interactions between the complexes and polyelectrolyte may induce changes in the excited state properties possibly due to electrostatic association, which is more sensitive to the charge of the metal ion, ligand

hydrophobicity and size of the complex. An observed increase in emission intensity is associated with electrostatic interaction. The binding constant determined for the complexes **3** to **8** were 1.3 X 10^4 M^{-1}, 8.5 X 10^4 M^{-1}, 3.8 X 10^4 M^{-1}, 1.7 X 10^4 M^{-1}, 1.6 X 10^4 M^{-1} and 2.3 X 10^4 M^{-1}. The binding constant K values were of the order **4>5>8>7>6>3**, consistent with the findings obtained from UV-visible spectral studies. The fluorescence emission spectrum of the ligands in the absence and presence of CT-DNA for the compounds **1** to **8** are given in Figs. 4.21a-d respectively[40]. The stern volmer plots are shown in Figs. 4.21b and 4.21f-h for the ligands and the complexes respectively.

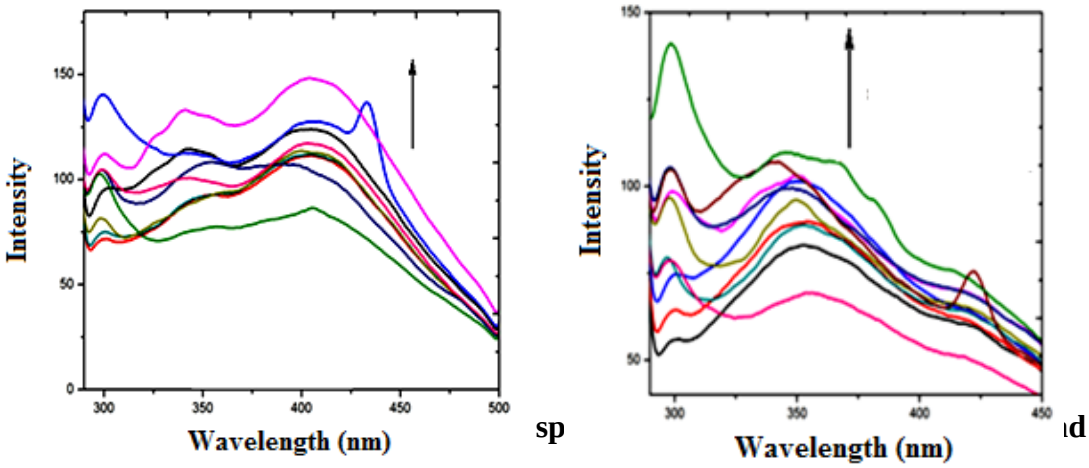

sp **ıd**

presence of CT-DNA. λex = 280nm.

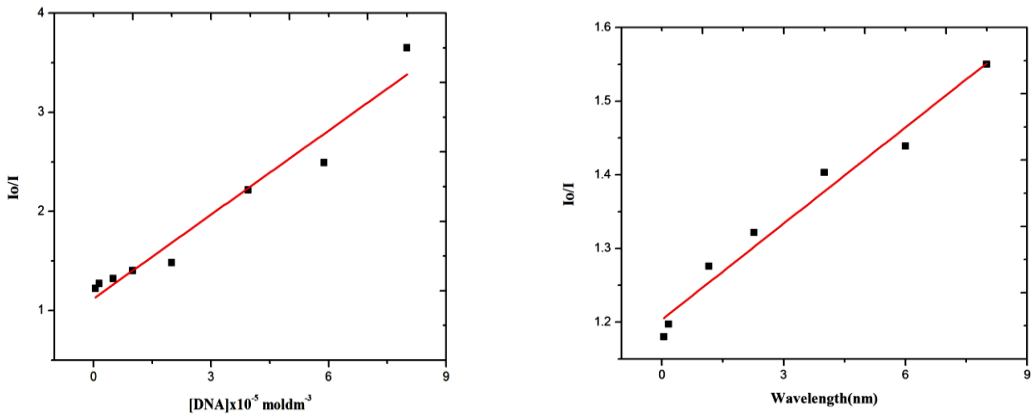

Fig. 4.21b. Stern volmer plot for the ligands 1 and 2

4.6.4. DNA Cleavage Studies

Chromosomal DNA fragmentation is caused by two types of DNA breaks *viz.*, single strand break and double strand breaks. Single strand cleavage of DNA has been suggested to occur during apoptosis while double strand DNA breaks are generally thought to have a greater biological consequence because they can lead directly to chromosomal aberrations and more frequently to the loss of genetic information. Double strand breaks are twenty times less frequent than single strand breaks and are more difficult to measure at physiological doses. DNA cleavage may be considered as an enzymatic reaction which comprises various biological processes as well as biotechnological manipulation of genetic material. It has wide applications in bioorganic chemistry, molecular biology and drug design. Metal containing reagents that induce chemical DNA scission are often referred to as artificial metallonucleases and the attention focused towards the development of new metallonucleases, which bind and cleave DNA at physiological conditions, have gained momentum

The interaction of plasmid pBr322 DNA with newly synthesized ligands and its Cu(II), Co(II) and Ni(II) complexes was studied using agarose gel electrophoresis method. The gel picture showing the cleavage of plasmid pBr322 DNA is depicted in Fig. 4.22. In the present study, the Ethidium bromide (EtBr) stained banding pattern of plasmid pBr322 DNA was tested with newly synthesized ligand and its metal complexes. In the present case, the Cu(II) complex with ligand **1**, Co(II) complex with ligand **1** showed complete cleavage of super coiled DNA and the Ni(II) complex showed partial cleavage of relaxed DNA and complete cleavage of supercoiled DNA. On the basis of these findings, it was concluded that all the newly synthesized compounds in the present study are good pathogenic microorganism inhibitor; as evident on the DNA cleavage of pBr322[41].

Complexes exhibit cleavage ability at low concentration (40 μM). When DNA is subjected to electrophoresis, relatively fast migration will be observed for the intact super coil form (Form I). If scission occurs on one strand (nicking), the super coil will relax to generate a slower moving open circular form (Form II). If both strands are cleaved, a linear form (Form III) that migrates between Forms-I and -II will be generated. From Fig. 4.22, it is evident all the complexes show more activity in the presence of oxidants which may be due to the reaction of hydroxyl radicals with DNA. These hydroxyl free radicals participate in the oxidation of the deoxyribose moiety followed by the hydroxyl cleavage of sugar phosphate backbone. In control experiment using DNA lane (1) no significant cleavage of DNA was observed even

after long exposure time. For the copper(II), nickel(II) and cobalt(II) complexes with ligand 1 (lane 3,6 and 7) Form I and Form II were observed. In the other complexes (lane 3 and 7), Form I, Form II and Form III were observed. The different cleavage efficiency of the complexes is due to the different binding efficiency of the complexes to DNA.

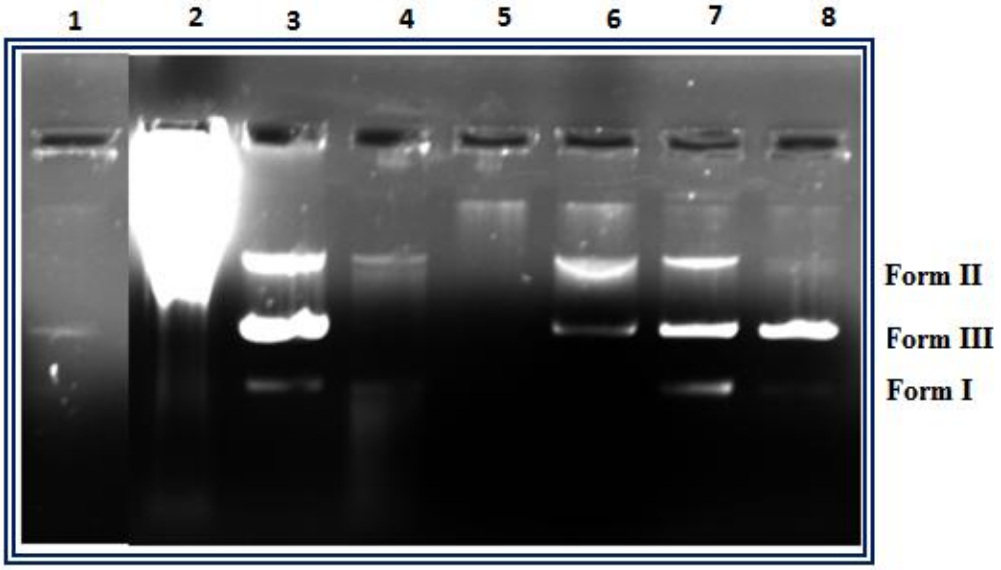

Fig.4.22. Changes in the agarose gel electrophoretic pattern of pBr322 DNA induced by H_2O_2 and metal complexes , lane 1, DNA alone; lane 2, DNA + H_2O_2; lane 3, DNA + 3+ H_2O_2; lane 4, DNA + 5 +H_2O_2; lane 5, DNA + 4 + H_2O_2; lane 6, DNA + 6 + H_2O_2; lane 7, DNA+8+H_2O_2, lane 8: DNA+7+H_2O_2

4. 6.5. Anti-tuberculosis activity

Tuberculosis is an infectious bacterial disease caused by *Mycobacterium tuberculosis*, most commonly affecting the lungs. According to World Health Organization, 8.8 million incident cases of TB were estimated globally in 2010. Treatment of drug resistant TB requires extensive chemotherapy with second line anti-tb drugs, which are costlier than first line drugs and produce severe adverse drug reactions[42]. The emergence of multidrug resistant strains highlighted the need for new drugs for the treatment of tuberculosis. The ligands **1** and **2** were checked for its anti-tuberculosis activity and the results are reported in table 4.19 and Fig. 4.23a. The strain used for this study was *M. tuberculosis* (H37 RV strain) and the standards (MIC values) used were Pyrazinamide (3.125μg/ml), Streptomycin (6.25 μg/ml), Ciprofloxacin (3.125 μg/ml). It is obvious from Table 4.19 that **1** has moderate

activity but **2** with the bromo substituent has a very low MIC value of 1.6 µg/ml, which is even lower than the tested standards and hence proved to be good against the bacterial strain. The anti-tuberculosis activity of the Ni(II) complex **6** (Fig. 4.23b) has been analysed and found to be 25 µg/ml which is a higher value than that of the ligands.

Table 4.19. MIC values in anti-tubercular activity

Compound	**100 µg/ml**	**50 µg/ml**	**25 µg/ml**	**12.5 µg/ml**	**6.25 µg/ml**	**3.12 µg/ml**	**1.6 µg/ml**	**0.8 µg/ml**
1	S	S	R	R	R	R	R	R
2	S	S	S	S	S	S	S	R
6	S	S	S	R	R	R	R	R

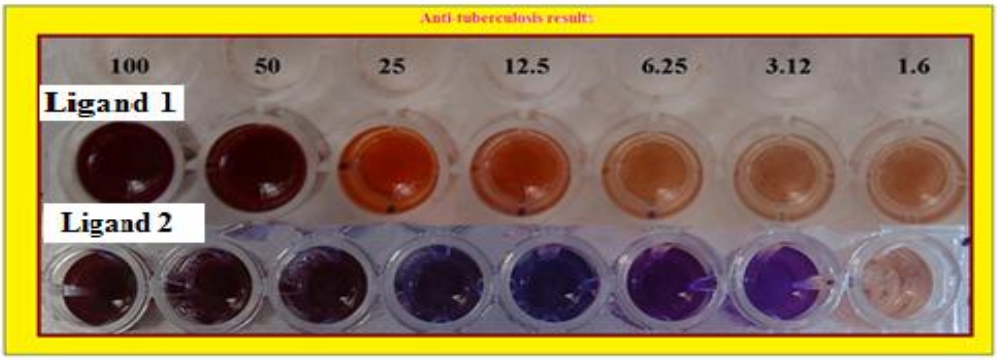

Fig. 4.23a. Anti-tubercular activity of ligands **1** and **2**

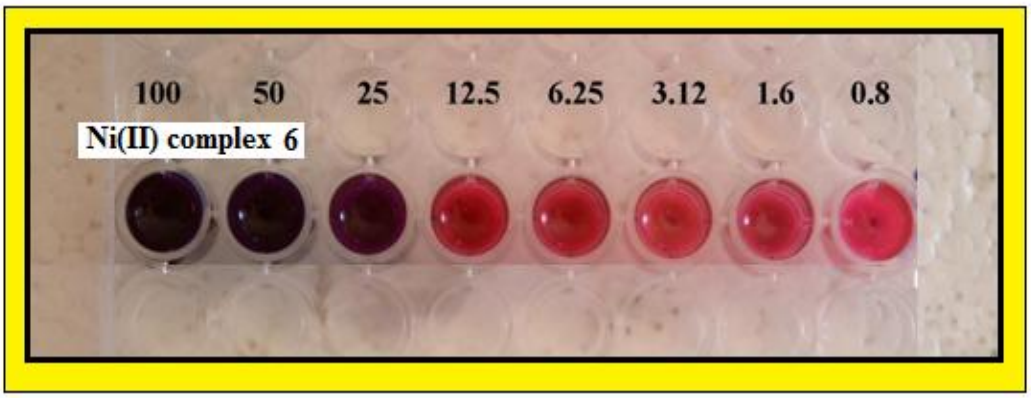

Fig. 4.23b. Anti-tubercular activity of the Ni(II) complex **6**

4.6.6. Complexation of β-Cyclodextrin with the Schiff bases

β-Cyclodextrin provides space for molecular encapsulation since it has a hydrophobic inner cavity and can tune the binding of compounds to DNA[43,44]. Hence, we studied the β-CD complex formation with the Schiff bases in solution using UV–

visible and fluorescence spectroscopy. The absorption spectrum of the ligand **1** consists of bands at 285 and 310 nm, corresponding to the π–π* and n–π* transitions respectively. The addition of β-CD in increasing concentrations from 0 to 1×10^{-2} mol dm^{-3} to the ligands **1** and **2** resulted in hyperchromic shifts of the absorption bands at 285 nm for **1** (Fig. 4.24a) and a hyperchromic shift along with a blue shift of about 20 nm (from 310 to 288 nm) for **2**. (Fig. 4.24b). This suggested that the pyrimidine moiety, responsible for the n–π* transition, got involved in the formation of a complex with β-CD. The calculated binding constants of the β-CD complexes of **1** and **2** were 3.08×10^5 and 1.9×10^4 M^{-2} respectively. The linearity in the plot suggested the formation of 1:1 complexes between the Schiff bases and β-CD.

The inclusion complex formation was further followed using fluorescence spectroscopy. The fluorescence bands were seen at 410 nm (for ligand **1**) and at 415 nm (for ligand **2**) in aqueous medium. Addition of β-CD in increasing concentrations from 0 to 1×10^{-2} mol dm^{-3} resulted in an enhancement of fluorescence of both the compounds (Figs. 4.24c and 4.24d). The above change was typical of the formation of inclusion complex between the guest molecules and β-CD. The Benesi–Hildebrand equation for the 1:1 binding is given by

$$\frac{1}{I - I_0} = \frac{1}{I' - I_0} + \frac{1}{I' - I_0}\frac{1}{K[\beta - CD]}$$

where Io, I, I' and K are the intensities of fluorescence of the fluorophore [ligands **1** and **2**] in water, intensity observed on varying the concentration of β-CD, intensity at the maximum concentration of β-CD, and the binding constant respectively. The stoichiometry of the inclusion complexes were 1 : 1 for both the compounds **1** and **2** (compound : β-CD) with the respective binding constants of 9.6×10^5 and 4.7×10^4 M^{-1}. This observation was in accordance with the results obtained in the absorption measurements[45-48]. The plots showing the linearity is shown from Figs. 4.24e and f respectively.

4.6.7. Docking

The crystal structure of the active sites was obtained from the protein data bank (PDB ID)-1: 1HVY, 2: 1VL, 3: 2FUM, 4: 3LPS, 5: 3TTZ, 6: 4FDR. The docking simulation was done using MOE software. All the conformers were docked at the defined cavity of the receptor. The glide energy and the docking scores are given as Table 4.20. The ligand forming the most stable drug receptor complex is the one having the least dock score value. The docking results reveal that the main

interaction force of the candidate compounds with the active sites is hydrophobic. The number of hydrophobic and hydrogen bonding interactions are given in Table 4.21.

Almost all the synthesized compounds are involved in at least two hydrogen bonding interaction with the active sites which is required for the activity[49]. The docking interactions of the Schiff bases with the active site are shown in Figs.4.25a to 4.25f respectively. The MIC values and the glide scores from the molecular docking studies do not have much correlation except the anti-tubercular protein which has better correlation.

4.7. Conclusion

The design and synthesis of novel pyrimidine Schiff base derivatives and their Cu(II), Co(II) and Ni(II) complexes bearing different substituents were carried out and the synthesized compounds were screened for their cytotoxic potency against human breast cancer cell line MCF-7 as well as their antimicrobial activities to check whether the compounds had any dual function anti-cancer/anti-microbial. The Schiff bases showed good activity against some of the bacterial and fungal strains under study. The anti-tubercular activity of the Schiff bases were studied and found to have pronounced activity for the bromo substituted compound than the tested standards. The molecular docking of the Schiff bases was done against six different active sites like Human Thymidylate synthase complexed with Dump and Raltitrex, crystal structure of Candida Albicans N-Myristoyl transferase peptidic inhibitor, catalytic domain of protein kinase pKnb from Mycobacterium tuberculosis in complex with Mitoxantrone, Crystal structure of Pare, crystal structure of Topoisomerase atpase inhibitor, crystal structure of E. coli and lactobacillus casdihydrofolate reductase. The Schiff bases and its complexes were studied for DNA binding through electrostatic mode in ligands and for complexes. The β-CD complexing ability of the ligands were studied and their binding constants were calculated. The DNA cleavage activity has been studied and the formations of two forms in the presence of hydrogen peroxide show that the mechanism is non-hydrolytic pathway. The compounds were

biologically active and if proven non-toxic they could be good lead compounds in medicinal chemistry.

References

1. Kandeel M M, Ali S M, Abed El Ali E K A, *Org Chem Indian J,* **9** (2013) 81.
2. Petrie C R, Cottam H B, Mckernan P A, *J Med Chem*, **28** (1985) 1010.
3. Baraldi P G, Pavani M G, Nunez M, *J Med Chem,* **10** (2002) 449.
4. Kandeel M M, Ali E K A, Abed El A, *J Chem Pharm Res,* **4** (2012) 4097.
5. Antre R V, Cendilkumar A, Goli D, *Saudi Pharm J,* 19 (2011) 233.
6. Mohammed M S, Kemel R, Fatahala S S, *Eur J Med Chem,* **45** (2010) 2994.
7. Yogesh K, Vinita G, Sanchita S, *J Pharm Res*, **7** (2013) 491.
8. Nagendar P, Malla Reddy G, Naresh Kumar R, *Bioorg Med Chem Lett,* **24**(2014) 2905.
9. Singh N P, Srivastava A N, *Asian J Chem,* **25** (2013) 533.
10. Maddila S, Kumar A S, Gorle S, *Lett Drug Design Discov*, **10** (2013) 186.
11. Xiaoling L, Mei-Liu G, *Bioorg Med Chem,* **14** (2006) 153.
12. Tarafder M T, Kasbollah A, Saravan N, *J Biochem Mol Biol Biophs,* **6** (2002) 85.
13. Hassanin H M, El-Edfawy S M, *Heterocycles*, **85** (2012) 2421.
14. Sharma S, Jain R, Sharma V, *J Indian Chem Soc,* **90** (2013) 221.
15. Gulcan M, Sonmez M, Berber I, *Turk J Chem,* **36** (2012) 189.
16. Kahveci B, Bekircan O , Karaoglu S A, *Indian J Chem*, **44B** (2005) 2614.
17. Betircan O, Kahveei B, Kucuk M, *Turk J Chem,* **30** (2006) 29.
18. Choudhari P B, Bhatia M S, Jadhav S D, *J Korean Chem Soc,* **57** (2013) 99.
19. Sheldrick, G.M (2008). *Acta Cryst.* A64, 112.
20. Dolomanov O V, Bourhis L J, Gildea R J, Howard J A K, Puschmann H, *J Appl Cryst*, **42**(2009) 339.
21. Trifunovic S R, Markoniv Z, Sladic D, *J Serb Chem Soc*,**67** (2002) 115.
22. Al-Shaalan N H, *Molecules,* **16** (2011) 8629.
23. Sonmez M, *Turk J Chem,* **25** (2001) 181.
24. Konstantinovic S S, Radovanovic B C, Cakiv Z, Vasic V, *J Serb Chem Soc*, **68** (2003) 641.
25. Bayoumi H A, Alaghaz A M A, *Int J Electrochem Sci,* **8** (2013) 9399.
26. Sallam S A, Ibrahim E S I, Anwar M I, *J Chil Chem Soc,* **57** (2012) 1482.

27. El-Baradie K Y, Gaber M, *Chem pap,* **57** (2003) 317.
28. Amer S, El-Wakiel N, El-Ghamry H, *J Mol Struct*, **1049** (2013) 326.
29. Russo M G, Narda G, E, *J Mol Struct,* **1061** (2014) 5.
30. Datta P, Sinha C, *Indian J Chem*, **48A** (2009) 1204.
31. Ayhan O, Zulbiye K, Murat S, Fatma K, *Chem Sci Rev Lett*, **4** (2015) 719.
32. Hatem M, Sheriff M S, Ibrahim S, *Acta Chim Slov*, **57** (2010) 230.
33. Durgadevi D, Dhandapani A, Manivarman, Subashchandrabose, *Can chem. Trans*, **4** (2016) 99.
34. Azantha P, Tinbaye A, Ponchaname, *Asian J Chem*, **28** (2016) 971.
35. Jone Kirubavathy S, Velmurugan R, Parameswari K, Chitra S, *IJPSR*, **5** (2014) 2508.
36. Sheikh J, Junieja H, Ingle V, Hadda T B, *J Saudi Chem Soc*, **17** (2013) 269.
37. Sameena Y, Enoch I V M V, *J. Lumin*, **138** (2013) 105.
38. Yousuf S , Enoch I V M V, *AAPS Pharm Sci Tech*, **14**(2013) 770.
39. Klymchenko A S, Shvadchak V V, Yushchenko D A, *J Phys Chem B,* **112** (2008) 12050.
40. Sameena Y, Ritty A, Selvakumar P M, *Chem Open* (2015) DOI: 10.1002/open.201500034.
41. Sathiyaraj S, Ayyanan G, Jayabalakrishnan C, *J Serb Chem Soc*, **79** (2014) 151.
42. Desai N C, Kotadiya G M, Trivedi A R, *Bioorg Med Chem Lett*, **24**(2014) 3126.
43. Yousuf S, Sudha N, *Carbohyd. Res*, **365** (2013) 46.
44. Lakowicz J R, Principles of fluorescence spectroscopy. Plenum Press: New York, (1999).
45. Chandrasekaran S, Sameena Y, Enoch I V M V, *J. Mol Recognit*, **27** (2014) 640.
46. Sameena Y, Sudha N, Chandrasekaran S, *J Biol Phys*, **40** (2014) 347.
47. Sowrirajan C, Yousuf S, Enoch I V M V, *Aust J Chem*, 67 (2014) 256.
48. Enoch I V M V, Yousuf S, *J Solution Chem*, **42** (2013) 470.
49. Ravichandiran P, Premnath D, Vasanthakumar S, *J Chem Biol*, **7** (2014) 122.